PHILOSOPHICAL TRANSACTIONS OF THE ROYAL SOCIETY A MATHEMATICAL, PHYSICAL & ENGINEERING SCIENCES

Magnetic Field Evolution in Steady Chaotic Flows

Andrew D. Gilbert

Phil. Trans. R. Soc. Lond. A 1992 **339**, 627-656
doi: 10.1098/rsta.1992.0053

Magnetic field evolution in steady chaotic flows

By Andrew D. Gilbert

Department of Applied Mathematics and Theoretical Physics, Silver Street, Cambridge CB3 9EW, U.K.

Contents

The fast dynamo problem for steady chaotic flows is approached by evolving magnetic field numerically at zero magnetic diffusion. Two flows are used, an *ABC* flow and a model flow constructed by patching simple flows together; both flows possess chaotic webs. From smooth initial conditions the magnetic field evolves fine structure in the chaotic regions of the flow because of exponential stretching and folding. Evidence for constructive folding of magnetic field within the chaotic regions is obtained: spatial averages of the magnetic field grow exponentially in time and this process is robust to different methods of averaging. This constructive folding is suggestive of fast dynamo action since the main effect of weak diffusion is to average field locally and smooth out fine variations. The growth and behaviour of initial conditions belonging to different symmetry classes is explored. In the case of the model flow, the dynamo process is explained in terms of chaotic stretching and folding together with cutting and pasting at hyperbolic stagnation points.

1. Introduction

It is now generally accepted that dynamo theory provides an explanation for the existence and dynamical behaviour of solar and terrestrial magnetic fields (see, for example, Moffatt 1978; Parker 1979; Krause & Rädler 1980); however, there remain a number of outstanding questions. One problem is to understand why the solar magnetic field evolves so rapidly, over a period of months for sunspots, or years for the solar cycle (Vainshtein & Zeldovich 1972). This timescale is that of the

Phil. Trans. R. Soc. Lond. A (1992) **339**, 627–656
Printed in Great Britain

convecting plasma in the sun, and is much shorter than the timescale for the diffusion of magnetic field across the solar convection zone, which is of the order of millions of years (Zeldovich *et al.* 1983). The apparent paradox is that diffusive processes must be important in allowing field lines to reconnect in any dynamo model, and yet the solar field evolves on a convective, rather than a diffusive, timescale. Dynamos with this property have been called 'fast dynamos' by Vainshtein & Zeldovich (1972). The resolution of the paradox is that convection tends to intensify the field and reduce its scale, which allows diffusion to act more rapidly, smoothing out fine structure and reconnecting field lines on small scales.

The fast dynamo problem then is to find examples of flows that are fast dynamos and to understand possible fast dynamo mechanisms. The problem is most easily approached within the framework of kinematic dynamo theory: one sets aside the effect of the Lorentz force on the convecting fluid and studies the evolution of magnetic field in a prescribed velocity field $\boldsymbol{u}(\boldsymbol{x}, t)$ according to the induction equation,

$$\partial_t \boldsymbol{B} = \nabla \times (\boldsymbol{u} \times \boldsymbol{B}) + \eta \nabla^2 \boldsymbol{B}, \tag{1}$$

with $\nabla \cdot \boldsymbol{B} = 0$. The magnetic diffusivity is η and we are interested in the limit of weak diffusion, $\eta \to 0$, for a given flow field. This is equivalent to the limit of large magnetic Reynolds number R_m; we use units in which the space-scales and timescales of the flow $\boldsymbol{u}$ are of order unity and take $R_\mathrm{m} \equiv 1/\eta$. If the flow is sufficiently complicated and extended in space, it will generally support dynamo action (Roberts 1972), the fastest growing magnetic field mode having a growth rate $p_{\max}(\eta)$. The flow $\boldsymbol{u}(\boldsymbol{x}, t)$ is a fast dynamo if

$$\lim_{\eta \to 0} \mathrm{Re}\, p_{\max}(\eta) > 0;$$

the growth rate remains on an $O(1)$ convective timescale in the limit of weak diffusion. If the limit is zero, the dynamo is slow.

Consider setting the diffusivity, η, exactly to zero so that magnetic field lines are frozen in the fluid. If the flow $\boldsymbol{u}$ is chaotic, field vectors are stretched exponentially and the scale of the field decreases exponentially without limit. For a flow in a bounded or periodic domain, this stretching of field must be accompanied by folding, a non-local effect that is difficult to quantify, yet is crucial in fast dynamos. The reason is that if one now introduces very weak diffusion, it will tend to smooth the field locally and the result of this smoothing process depends on the nature of the folding that has taken place. If the folding is 'constructive' in the sense that largely like-signed field is brought together, then the effect of diffusion in dissipating magnetic energy is minimized. Therefore, at a heuristic level at least, the question of whether a chaotic flow is a fast dynamo becomes a question of the nature of folding in three-dimensional flows (see Dresselhaus & Tabor 1990).

The fast dynamo problem has been approached by the study of idealized models and the numerical study of 'realistic' flows. We take a rather weak definition of a realistic flow as one that lies in bounded or periodic three-dimensional space, and stretches fluid elements by only finite amounts over finite periods of time; this excludes examples of laminar fast dynamos in which fluid elements are literally torn apart by singularities in the flow field (Soward 1987; Gilbert 1988). Among the idealized models are examples of smooth flows on compact manifolds in which the folding is always constructive (Arnold *et al.* 1981; Bayly 1986; Vishik 1989); however, it may be impossible to realize these flows in ordinary space (Plante & Thurston 1972). Other idealized models capture fast dynamo mechanisms which may

PHILOSOPHICAL TRANSACTIONS OF THE ROYAL SOCIETY A MATHEMATICAL, PHYSICAL & ENGINEERING SCIENCES

be present in realistic flows; these include the stretch–twist–fold mechanism (Vainshtein & Zeldovich 1972; Finn & Ott 1988, 1990) and stretch–fold–shear mechanism (Soward 1987; Bayly & Childress 1988, 1989; Finn *et al.* 1991). There is convincing numerical evidence for fast dynamo action in realistic unsteady flows (Bayly & Childress 1988; Finn & Ott 1988; Otani 1989; Klapper 1992*b*; Galloway & Proctor 1992) and random flows (see, for example, Zeldovich *et al.* 1988 and references therein).

In this paper we are concerned with realistic steady chaotic flows; it has been suggested that these are typically fast dynamos (Finn *et al.* 1991). Studies have largely focused on the *ABC* flows (Arnold 1965; Childress 1970):

$$\boldsymbol{u}(\boldsymbol{x}) = (C\sin z + B\cos y, A\sin x + C\cos z, B\sin y + A\cos x). \tag{2}$$

This is a family of smooth periodic flows of maximal fluid helicity (Moffatt 1969) given by three parameters, A, B and C. Except in cases where one or more of these parameters is zero, the flow is non-integrable and possesses regions of chaotic streamlines mingled with 'tubes' of quasi-periodic streamlines (Hénon 1966; Dombre *et al.* 1986). Dynamo action in certain non-integrable *ABC* flows has been studied numerically for $R_{\mathrm{m}} \leqslant 550$ (Arnold & Korkina 1983; Galloway & Frisch 1986); the results are perhaps suggestive of fast dynamo action, but as yet inconclusive. More convincing evidence for fast dynamo action in a steady Kolmogorov flow has been obtained recently by Galloway & Proctor (1992). Such numerical simulations are expensive since the magnetic field is three dimensional and has structure down to diffusive scales of $O(R_{\mathrm{m}}^{-\frac{1}{2}})$ (Moffatt & Proctor 1985).

Our approach is to follow the evolution of magnetic fields in examples of steady flows with zero magnetic diffusivity. We identify constructive folding in the flow by calculating the average field over fixed regions of space. If the average grows exponentially it indicates constructive folding, which is suggestive of fast dynamo action, since the principal effect of diffusion is to average the field over fine scales (Finn & Ott 1988; Vishik 1989). This idea of replacing diffusion by averaging can be made precise and proved in a number of idealized models (Bayly & Childress 1989; Finn *et al.* 1991; Childress & Klapper 1991; Klapper 1992*a*, *b*). For a steady flow containing a mixture of islands and chaos, there are difficulties in making a rigorous link. In this paper we do not address this delicate issue directly, but simply seek evidence for constructive folding in steady chaotic flows at zero magnetic diffusivity.

The paper falls naturally into two parts. In the first part (§§2–7) our aim is to study magnetic field evolution in the simplest possible realistic flow. We construct a flow, based loosely on a nearly integrable *ABC* flow (§2), by patching together simple flows; this is called the '*ABCS*' flow for brevity (§3). The flow is constructed in such a way that particles and magnetic field vectors can be evolved in time using discrete maps (§4) without approximation. This is numerically efficient and enables us to study constructive folding and fast dynamo mechanisms in considerable detail (§§5–7). In the second part (§§8 and 9) we return to the original *ABC* family (2) and study the flow with $A = B = C = 1$. Finally, in §10 we offer discussion and conclusions. Some of the results in this paper have been reported in Gilbert & Childress (1990) and Gilbert (1991).

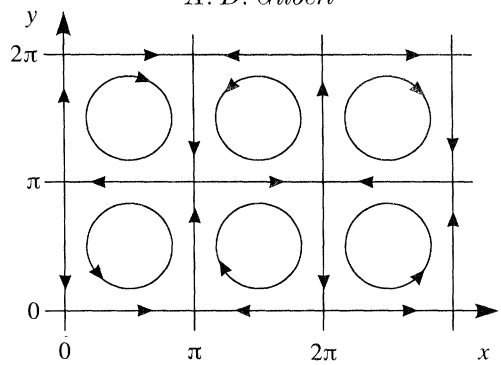

Figure 1. Streamlines of the ABC flow with $A = B$ and $C = 0$, projected onto the xy plane.

2. A map for nearly integrable ABC flows with $A = B = 1, C \ll 1$

In this section we consider nearly integrable ABC flows with $A = B = 1$ and $C \ll 1$ and derive a map giving particle trajectories. After applying a rotation, a dilation and a translation to (2) with $A = B = 1$, the flow takes the form

$$\boldsymbol{u} = (\Phi_y, -\Phi_x, \Phi\sqrt{2}) + C(\cos(z\sqrt{2}), -\sin(z\sqrt{2}), 0), \tag{3}$$

where $\Phi(x, y) = \sin x \sin y$. When C is zero the flow is integrable and Φ is a streamfunction for the motion projected onto the xy plane. The projected flow is shown schematically in figure 1 and comprises a periodic array of cells. There is a lattice of X-type, or hyperbolic, stagnation points, $\pi\boldsymbol{n} \equiv \pi(n_x, n_y, 0)$, where n_x and n_y are integers, joined by a network of separatrices, or heteroclinic streamlines. When C is increased from zero the z-dependent Beltrami wave perturbs the separatrices so that they no longer exactly connect the stagnation points. The network of separatrices broadens into a network of chaotic layers of width $O(C)$, which form a chaotic web (Zaslavsky *et al.* 1988; Beloshapkin *et al.* 1989). We shall derive a map giving the motion of particles in this flow using standard methods in hamiltonian systems (Chirikov 1979) and following from the discussion of Zaslavsky *et al.* (1988). We shall see that this map is not entirely suitable for fast dynamo studies, but we discuss it here as it forms a basis for the patched $ABCS$ flow which we introduce in §3 and use extensively in the paper.

To obtain equations for the motion of a particle in the web it is appropriate to scale $\Phi = O(C)$ for $C \ll 1$. The velocity of the particle in the z direction is then $O(C)$ and it turns out that to leading order z is constant; the small changes in z may be calculated later. We approximate the motion near to stagnation points, and along the perturbed separatrices. Near to the stagnation point at the origin take $x, y \approx O(\sqrt{C})$ and $\Phi \approx xy$. The effect of the perturbation is negligible here, since the streamlines are relatively far apart and the flow is slow moving. Thus on a trajectory $\Phi \approx \phi_0$, where ϕ_0 is an $O(C)$ constant. The equations of motion for a particle are

$$\dot{x} = x, \quad \dot{y} = -y, \tag{4}$$

and an orbit is given by

$$x = \sqrt{|\phi_0|}\exp(t - t_0), \quad y = \sqrt{|\phi_0|}\,\mathrm{sign}(\phi_0)\exp(t_0 - t),$$

where the subscript 0 gives values of Φ and t when the orbit crosses either of the lines $x = \pm y$. Near to the stagnation point $(x, y) = (\pi, 0)$, $\Phi \approx \phi_2$ on a trajectory and

$$x = \pi - \sqrt{|\phi_2|}\exp(t_2 - t), \quad y = \sqrt{|\phi_2|}\,\mathrm{sign}(\phi_2)\exp(t - t_2),$$

where the subscript 2 denotes values when $x - \pi = \pm y$.

Near the unperturbed separatrix joining these two stagnation points, scale $x = O(1)$ and $y = O(C)$, so that $\Phi \approx y \sin x$ and a particle moves according to

$$\dot{x} = \sin x, \quad \dot{y} = -y \cos x - C \sin (z\sqrt{2}), \tag{5}$$

the perturbation being important in this region. Since z is constant at leading order, these equations give

$$x = 2 \arctan [\exp (t - t_1)], \quad y = \cosh (t - t_1)(\phi_1 + (x - \tfrac{1}{2}\pi)(-C \sin (z\sqrt{2}))),$$

where the subscript 1 denotes the values of Φ and t when $x = \frac{1}{2}\pi$. Matching the three approximations relates values of Φ and t near the two stagnation points:

$$\phi_2 - \phi_0 = -C\pi \sin (z\sqrt{2}), \quad t_2 - t_0 = \tfrac{1}{2}(T(\phi_2) + T(\phi_0)),$$

where $T(\phi) \equiv \ln (4/|\phi|)$.

Now let us determine the small changes in z, which are important for the existence of chaos in the flow; without these an orbit would always lie in a plane of constant z and undergo periodic or quasi-periodic motion (see Soward & Childress 1990). Using $\dot{z} = \sqrt{2\Phi}$ in the three regions and matching gives the total displacement in z as

$$z_2 - z_0 = \tfrac{1}{2}(\Delta(\phi_2) + \Delta(\phi_0)),$$

where $\Delta(\phi) \equiv \sqrt{2}\phi T(\phi)$. The displacement is $O(C \ln C)$, which is small, as assumed (Zaslavsky *et al.* 1988).

All the other separatrices and stagnation points are treated in a similar way and this leads to an approximate map for the motion of a particle from the neighbourhood of any stagnation point to the next in the flow. Using carets to indicate new values of variables we obtain the map:

$$\left.\begin{aligned} &\hat{\phi} = \phi + \pi p(z, \boldsymbol{e}), \quad \hat{z} = z + \tfrac{1}{2}(\Delta(\hat{\phi}) + \Delta(\phi)), \\ &\hat{t} = t + \tfrac{1}{2}(T(\hat{\phi}) + T(\phi)), \\ &\hat{\boldsymbol{n}} = \boldsymbol{n} + \boldsymbol{e}, \quad \hat{\boldsymbol{e}} = (\boldsymbol{e}_z \times \boldsymbol{e}) \operatorname{sign} (\hat{\phi}). \end{aligned}\right\} \tag{6}$$

The map describes a particle which moves from the neighbourhood of the stagnation point $\pi\boldsymbol{n}$ in the direction $\boldsymbol{e} = \pm\boldsymbol{e}_x$ or $\pm\boldsymbol{e}_y$ to the stagnation point $\pi\hat{\boldsymbol{n}}$. The values of ϕ, z and t are those when the particle crosses one of the surfaces $x - \pi n_x = \pm (y - \pi n_y)$, which we refer to as Poincaré sections, and similarly for $\hat{\phi}$, $\hat{z}$, $\hat{t}$ and $\hat{\boldsymbol{n}}$. The function p is defined by

$$p(z, \boldsymbol{e}) \equiv -C\boldsymbol{e} \cdot (\sin (z\sqrt{2}), \cos (z\sqrt{2}), 0). \tag{7}$$

There is an immediate problem with this map as written: although it arises from a solenoidal flow, it does not preserve fluid volumes. This can be seen in numerical simulations, or shown informally as follows. At a point (ϕ, z) on a section, an element of area may be defined by displacements $\mathrm{d}\phi, \mathrm{d}z$ on the section; this can be extended into an element of volume by carrying the area element along streamlines (assumed transverse to the section) for a short time $\mathrm{d}t$. The volume of this infinitesimal element is then $V(\phi, z)\,\mathrm{d}\phi\,\mathrm{d}z\,\mathrm{d}t$ for some function V and must be conserved under the Poincaré map for a solenoidal flow. The jacobian of the mapping must therefore take the form:

$$\partial(\hat{\phi}, \hat{z}, \hat{t})/\partial(\phi, z, t) = V(\phi, z)/V(\hat{\phi}, \hat{z}).$$

The jacobian of (6) cannot be written in this form and therefore is not the Poincaré map of a solenoidal flow. This problem is easily rectified by noting that in working

out the change in ϕ, z was taken as an $O(1)$ quantity; to this order one could equally well use $\hat{z}$ or any quantity which differs from z by an amount of less than $O(1)$. To obtain a volume-preserving map, we instead write:

$$\hat{\phi} = \phi + \pi p(z + \tfrac{1}{2}\Delta(\phi), \boldsymbol{e});$$

With this change the jacobian of the Poincaré map now has determinant 1 and so corresponds to a solenoidal flow.

This map gives a description of how particles move from stagnation point to stagnation point in the chaotic web. Some particles wander randomly around the network of separatrices, whereas others have a systematic motion in a given direction or remain trapped in one cell of the structure (Beloshapkin *et al.* 1989). Note that the change of variables

$$\psi = \phi + \tfrac{1}{2}\pi p(\zeta, \boldsymbol{e}), \quad \psi_X = \hat{\phi},$$
$$\zeta = z + \tfrac{1}{2}\Delta(\phi), \quad \tau = t + \tfrac{1}{2}T(\phi),$$

gives a map that moves particles from the centre of one separatrix layer to the next:

$$\left.\begin{aligned} \hat{\psi} &= \psi_X + \tfrac{1}{2}\pi p(\hat{\zeta}, \hat{\boldsymbol{e}}), \quad \psi_X = \psi + \tfrac{1}{2}\pi p(\zeta, \boldsymbol{e}), \\ \hat{\zeta} &= \zeta + \Delta(\psi_X), \quad \hat{\tau} = \tau + T(\psi_X), \\ \hat{\boldsymbol{n}} &= \boldsymbol{n} + \boldsymbol{e}, \quad \hat{\boldsymbol{e}} = (\boldsymbol{e}_z \times \boldsymbol{e}) \operatorname{sign}(\psi_X). \end{aligned}\right\} \tag{8}$$

Here ψ and τ are the values of Φ and t when a particle crosses a Poincaré section, these now being placed across the middle of each separatrix layer; ψ_X is the value of Φ near the next stagnation point.

This map moves particles in the model flow and its jacobian can be used to move vectors (see §4). To find the field at a point one could follow the orbit back from that point using the map, pick up the initial field and transport it forwards along the orbit using the Cauchy solution. However, there are some difficulties in using the map for numerical fast dynamo studies. If one follows a particle back in time it generally lands somewhere between the Poincaré sections used in the map and its position is only known in terms of matched approximations. If these are implemented in a numerical code up to a given order in C, there will inevitably be errors at the next order, which may introduce unphysical effects such as the cutting of magnetic field lines, violating $\nabla \cdot \boldsymbol{B} = 0$. This could make the unambiguous identification of constructive folding and fast dynamo action difficult. Another effect of making the above approximations is to change the qualitative structure of the flow. For example in the real ABC flow with $A = B = 1$ and $C \ll 1$ there are a finite number of discrete hyperbolic stagnation points in each periodicity box (Dombre *et al.* 1986), whereas in the approximation there are whole lines of stagnation points, a degenerate situation.

3. Description of the *ABCS* flow

There are certain difficulties in using the approximate map (8), derived from a nearly integrable ABC flow, for fast dynamo studies. Instead we construct a flow, called the '$ABCS$' flow, which is loosely based on the ABC flow with $A = B = 1$, $C \ll 1$. The flow is defined by taking the leading order approximations to this ABC flow near to stagnation points and separatrices, and patching these together. Divide

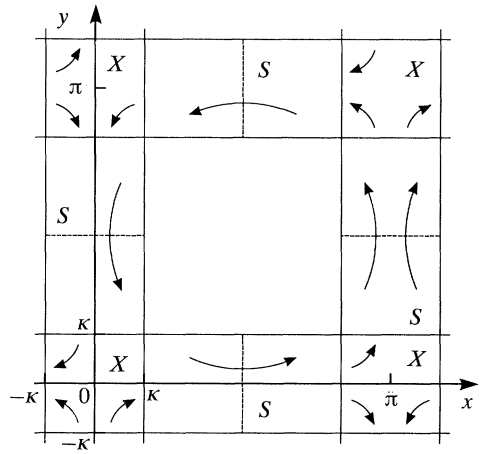

Figure 2. Structure of the model flow. The figure shows the projection on the xy plane of the periodic array of regions labelled S and X. The Poincaré section across each S-region is marked by a dashed line.

space into regions labelled 'X', containing X-type or hyperbolic, stagnation points, connected by regions labelled 'S', standing for 'separatrix', as shown in figure 2. In an X-region the flow is essentially the stagnation point flow (4), together with vertical motion, while in an S-region the flow is given by (5) and no vertical motion. Particle trajectories in this flow can be integrated analytically to give a map, which can then be used to evolve magnetic field efficiently on a computer. Note that the $ABCS$ flow is not a rational approximation to any ABC flow, but merely has certain features in common.

Precise details follow; the regrettably cumbersome notation will be needed for explaining in §4 how magnetic field is evolved in the flow. For a terse description see Gilbert & Childress (1990). The flow, projected onto the xy plane (figure 2), has stagnation points at $\pi\boldsymbol{n} \equiv \pi(n_x, n_y, 0)$ where n_x and n_y are integers. Centred at each stagnation point lies an 'X-region', a square of side 2κ, where κ is a fixed parameter. Joining the X-regions are 'S-regions', which we discuss first; these are rectangles of the form:

$$S(\boldsymbol{n}, \boldsymbol{e}) \equiv \{\boldsymbol{x} : \kappa < \boldsymbol{e}\cdot(\boldsymbol{x}-\pi\boldsymbol{n}) < \pi-\kappa, |(\boldsymbol{e}_z \times \boldsymbol{e})\cdot(\boldsymbol{x}-\pi\boldsymbol{n})| < \kappa\}.$$

The S-region $S(\boldsymbol{n}, \boldsymbol{e})$ lies between the stagnation points at $\pi\boldsymbol{n}$ and $\pi(\boldsymbol{n}+\boldsymbol{e})$. The unit vector $\boldsymbol{e}$ gives the general direction of flow in the region as shown in figure 2 and so $\boldsymbol{e} = \pm\boldsymbol{e}_x$ if the sum of the components of $\boldsymbol{n}$ is even and $\boldsymbol{e} = \pm\boldsymbol{e}_y$ if the sum is odd. To describe the flow it is convenient to introduce 'local coordinates' $(\bar{x}, \bar{y}, \bar{z}, \boldsymbol{n}, \boldsymbol{e})$ by writing

$$\boldsymbol{x} = M_{\mathrm{CL}}(\bar{x}, \bar{y}, \bar{z}, \boldsymbol{n}, \boldsymbol{e}) \equiv \pi\boldsymbol{n} + \bar{x}\boldsymbol{e} + \bar{y}\boldsymbol{e}_z \times \boldsymbol{e} + \bar{z}\boldsymbol{e}_z, \tag{9}$$

so that

$$S(\boldsymbol{n}, \boldsymbol{e}) \equiv \{(\bar{x}, \bar{y}, \bar{z}, \boldsymbol{n}, \boldsymbol{e}) : \kappa < \bar{x} < \pi-\kappa, |\bar{y}| < \kappa\}.$$

The flow in $S(\boldsymbol{n}, \boldsymbol{e})$ is defined to be

$$\partial_t(\bar{x}, \bar{y}, \bar{z}) = (\partial_{\bar{y}}\, \Psi(\bar{x}, \bar{y}), -\partial_{\bar{x}}\, \Psi(\bar{x}, \bar{y}) + p(\bar{z}, \boldsymbol{e}), 0),$$

where $\Psi(\bar{x}, \bar{y}) \equiv \bar{y}\sin\bar{x}$ and $p(z, \boldsymbol{e})$ was defined in (7). Here Ψ is the unperturbed $C = 0$ streamfunction which it is often convenient to use as a spatial coordinate. The

function p represents the effect of the perturbing Beltrami wave $C(\cos(z\sqrt{2}), -\sin(z\sqrt{2}), 0)$ in pushing particles across the lines of constant Ψ in the $\bar{y}$ direction. When a particle traverses an S-region the change in Ψ is $2q$, where

$$q(\bar{z}, \boldsymbol{e}) \equiv (\tfrac{1}{2}\pi - \kappa)\, p(\bar{z}, \boldsymbol{e}),$$

and there is no vertical displacement. The time taken,

$$T_S \equiv -2 \ln(\tan \tfrac{1}{2}\kappa),$$

is the same for all particles.

Now define X-regions $X(\boldsymbol{n}, \boldsymbol{e})$ by

$$X(\boldsymbol{n}, \boldsymbol{e}) \equiv \{\boldsymbol{x} : \pi - \kappa < \boldsymbol{e} \cdot (\boldsymbol{x} - \pi\boldsymbol{n}) < \pi + \kappa, |(\boldsymbol{e}_z \times \boldsymbol{e}) \cdot (\boldsymbol{x} - \pi\boldsymbol{n})| < \kappa\},$$

where again $\boldsymbol{e}$ is restricted to be $\pm \boldsymbol{e}_x$ if $n_x + n_y$ is even, and $\pm \boldsymbol{e}_y$ otherwise. Note that $X(\boldsymbol{n}, \boldsymbol{e})$ is a square of side 2κ centred at $\pi(\boldsymbol{n} + \boldsymbol{e})$, rather than $\pi\boldsymbol{n}$. In local coordinates (9),

$$X(\boldsymbol{n}, \boldsymbol{e}) \equiv \{(\bar{x}, \bar{y}, \bar{z}, \boldsymbol{n}, \boldsymbol{e}) : \pi - \kappa < \bar{x} < \pi + \kappa, |\bar{y}| < \kappa\}.$$

The flow in an X-region is a stagnation point flow given by:

$$\partial_t(\bar{x}, \bar{y}, \bar{z}) = (\partial_{\bar{y}} \Psi(\bar{x}, \bar{y}), -\partial_{\bar{x}} \Psi(\bar{x}, \bar{y}), \sqrt{2}\Psi(\bar{x}, \bar{y})),$$

where $\Psi(\bar{x}, \bar{y}) = \gamma(\pi - \bar{x})\, \bar{y}$ is the unperturbed streamfunction in $X(\boldsymbol{n}, \boldsymbol{e})$. The constant $\gamma \equiv (\sin\kappa)/\kappa$ is defined to make Ψ continuous across the boundary between X- and S-regions; so that the flow conserves volume. Note, however, that there is a discontinuity in the angle of the streamlines (corresponding to a vortex sheet in the flow), and thus a fluid element crossing the boundary is stretched instantaneously by a finite amount. This discontinuity in angle could be smoothed out, so that this finite stretching would take place smoothly over a short time, without affecting our results in any significant way.

In an X-region a particle moves along a curve of constant Ψ; it spends a time

$$T_X(\Psi) \equiv \gamma^{-1} \ln|\gamma\kappa^2/\Psi|$$

in the region and undergoes a vertical displacement of

$$\Delta(\Psi) \equiv \sqrt{2}\Psi T_X(\Psi).$$

Note that, as in the approximation to the ABC flow of §2, the $ABCS$ flow is somewhat degenerate, as in each X-region there is a line of hyperbolic stagnation points, each with a neutral direction. The flow is now defined within X- and S-regions by two parameters, C and κ. These are chosen so that the chaotic web is contained entirely within X- and S-regions. Thus the flow need not be defined explicitly in the spaces outside these regions (see figure 2).

The flow may be integrated to obtain a Poincaré map. First we define a two-dimensional Poincaré section $P(\boldsymbol{n}, \boldsymbol{e})$ lying across the centre of each S-region $S(\boldsymbol{n}, \boldsymbol{e})$ by

$$P(\boldsymbol{n}, \boldsymbol{e}) = \{(\bar{x}, \bar{y}, \bar{z}, \boldsymbol{n}, \boldsymbol{e}) : \bar{x} = \tfrac{1}{2}\pi, -\kappa < \bar{y} < \kappa\};$$

these are shown by dashed lines in figure 2. The Poincaré map relates successive positions and times when a particle crosses a section. If a particle crosses $P(\boldsymbol{n}, \boldsymbol{e})$ at time $t = \tau$ with $z = \zeta$ and $\Psi = \psi$, this is recorded as $(\psi, \zeta, \tau, \boldsymbol{n}, \boldsymbol{e})$. The particle then travels along $S(\boldsymbol{n}, \boldsymbol{e})$ and into $X(\boldsymbol{n}, \boldsymbol{e})$. Here it moves along some streamline $\Psi = \psi_X$

PHILOSOPHICAL TRANSACTIONS OF THE ROYAL SOCIETY A MATHEMATICAL, PHYSICAL & ENGINEERING SCIENCES

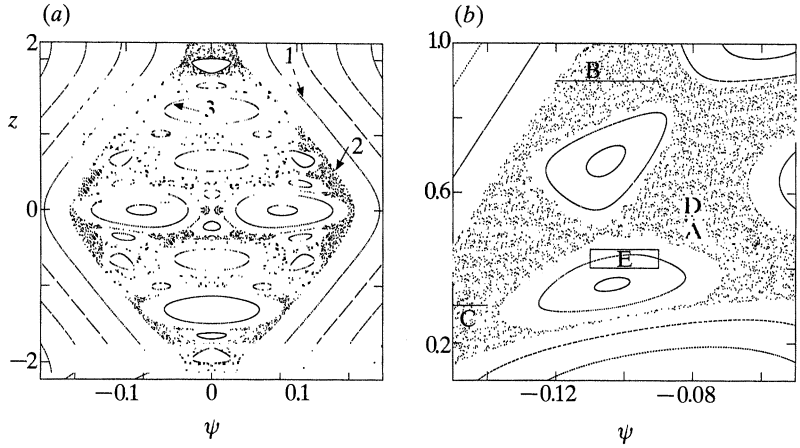

Figure 3. Streamlines of the model flow. In (*a*) the part of the Poincaré section $P(0, \boldsymbol{e}_x)$ given by $x = \frac{1}{2}\pi$, $|\psi| < 0.2$ and $|z| < \pi/\sqrt{2}$ is shown. Points are plotted where streamlines intersect this section, modulo the periodicity of the flow. The box marked in (*a*) is given by $-0.15 < \psi < -0.05$, $0.1 < z < 1$ and is enlarged in (*b*). The horizontal lines shown in (*b*) are given by A: $-0.09 < \psi < -0.07$, $z = 0.53$; B: $-0.12 < \psi < -0.09$, $z = 0.9$; and C: $-0.15 < \psi < -0.14$, $z = 0.3$. The boxes shown in (*b*) are given by D: $-0.09 < \psi < -0.07$, $0.54 < z < 0.6$; and E: $-0.11 < \psi < -0.09$, $0.4 < z < 0.45$.

and turns left if $\psi_X > 0$ or right if $\psi_X < 0$. It enters another S-region and intersects $P(\hat{\boldsymbol{n}}, \hat{\boldsymbol{e}})$ at

$$(\hat{\psi}, \hat{\zeta}, \hat{\tau}, \hat{\boldsymbol{n}}, \hat{\boldsymbol{e}}) = M_{PP}(\psi, \zeta, \tau, \boldsymbol{n}, \boldsymbol{e}),$$

where

$$\left.\begin{aligned} &\hat{\psi} = \psi_X + q(\hat{\zeta}, \hat{\boldsymbol{e}}), \quad \psi_X = \psi + q(\zeta, \boldsymbol{e}), \\ &\hat{\zeta} = \zeta + \Delta(\psi_X), \quad \hat{\tau} = \tau + T(\psi_X), \\ &\hat{\boldsymbol{n}} = \boldsymbol{n} + \boldsymbol{e}, \quad \hat{\boldsymbol{e}} = (\boldsymbol{e}_z \times \boldsymbol{e}) \operatorname{sign}(\psi_X). \end{aligned}\right\} \tag{10}$$

Here ψ_X is an intermediate variable, the value of Ψ in the X-region, and

$$T(\psi_X) \equiv T_S + T_X(\psi_X).$$

This map is the same as that derived for the ABC flow (8) in §2, except that $\frac{1}{2}\pi p$ is replaced by q, and the functions T and Δ are defined differently. By iterating this map particles may be moved efficiently and accurately from section to section and by using the detailed structure of the flow the exact position of a particle may be determined at any time.

For all our numerical studies $C = 0.1$ and $\kappa = \sqrt{0.5}$. The Poincaré map contains information about the motion of the particle on the large-scale lattice, given by $\boldsymbol{n}$, as well as the motion on small scales given by ψ, ζ, τ and $\boldsymbol{e}$. To give a picture of the small-scale structure we identify all points modulo the periodicity of the flow and plot part of the Poincaré section $P(0, \boldsymbol{e}_x)$ in figure 3*a*. There are three types of orbit visible; examples are labelled (1), (2) and (3). The orbit (1) undergoes a spiralling motion and is confined to just one cell in the network; it is essentially a slightly perturbed streamline of the $C = 0$ integrable system. However, an orbit such as (2) lies in the chaotic web formed by the perturbed $C = 0$ separatrices. It is chaotic and appears to fill areas of space on the section. On large scales it wanders around the lattice of S- and X-regions in a chaotic manner. The orbit (3) lies inside the web but is quasiperiodic, tracing out an island on the section, while on large scales it has a persistent motion through the lattice.

4. The Cauchy solution

When the magnetic diffusion in the induction equation (1) is zero, a magnetic field evolves according to the Cauchy solution:

$$\boldsymbol{B}(\boldsymbol{x},t) = \partial\boldsymbol{x}/\partial\boldsymbol{x}_0 \cdot \boldsymbol{B}(\boldsymbol{x}_0,0). \tag{11}$$

Here $\boldsymbol{x}_0(\boldsymbol{x},t)$ is the initial position of the fluid element which lies at $\boldsymbol{x}$ at time t. The Poincaré map moves particles from section to section through the flow; however, generally a particle will not lie on a Poincaré section at time 0 or t and some interpolation is needed. Suppose, then, that a particle crosses $P(\boldsymbol{n},\boldsymbol{e})$ at position and time $(\psi,\zeta,\tau,\boldsymbol{n},\boldsymbol{e})$. Provided $|t-\tau| < \frac{1}{2}T_S$, so that it is still in $S(\boldsymbol{n},\boldsymbol{e})$ at time t, its position at this time is given in local coordinates by

$$(\bar{x},\bar{y},\bar{z},\boldsymbol{n},\boldsymbol{e}) = M_{LP}^{(t)}(\psi,\zeta,\tau,\boldsymbol{n},\boldsymbol{e}),$$

where
$$\bar{x} = a(t-\tau), \quad \bar{y} = b(t-\tau)\,c(\psi,\zeta,t-\tau,\boldsymbol{e}), \quad \bar{z} = \zeta,$$

with
$$a(t) \equiv 2\arctan[\exp t], \quad b(t) \equiv \cosh t,$$

$$c(\psi,\zeta,t,\boldsymbol{e}) \equiv \psi + (a(t)-\tfrac{1}{2}\pi)\,p(\zeta,\boldsymbol{e}).$$

Again consider motion from $\boldsymbol{x}_0$ to $\boldsymbol{x}$ over some period of time t, and suppose that both $\boldsymbol{x}_0$ and $\boldsymbol{x}$ lie in S-regions; there are trivial modifications if one or both of these points lies in an X-region, which are summarized in Appendix A. Then

$$\boldsymbol{x}(\boldsymbol{x}_0) = M_{CL} \circ M_{LP}^{(t)} \circ (M_{PP})^n \circ (M_{LP}^{(0)})^{-1} \circ (M_{CL})^{-1}(\boldsymbol{x}_0), \tag{12}$$

where $\circ$ means the composition of maps. Essentially we move the particle from $\boldsymbol{x}_0$ to the nearest Poincaré section, iterate M_{PP} n times to move it from section to section, and obtain its final position.

Differentiating (12) at fixed time t, using the chain rule, gives the jacobian $\partial\boldsymbol{x}/\partial\boldsymbol{x}_0$ as the product of jacobians of maps:

$$\partial\boldsymbol{x}/\partial\boldsymbol{x}_0 = \boldsymbol{J}_{CL}\cdot\boldsymbol{J}_{LP}^{(t)}\cdot(\boldsymbol{J}_{PP})^n\cdot(\boldsymbol{J}_{LP}^{(0)})^{-1}\cdot(\boldsymbol{J}_{CL})^{-1} \tag{13}$$

(whose arguments are omitted for brevity). The jacobians of the maps $M_{LP}^{(t)}$ and M_{CL} are

$$\boldsymbol{J}_{LP}^{(t)} = \frac{\partial(\bar{x},\bar{y},\bar{z})}{\partial(\psi,\zeta,\tau)} = \begin{pmatrix} 0 & 0 & -a' \\ b & bp'(a-\frac{1}{2}\pi) & -cb'-p \\ 0 & 1 & 0 \end{pmatrix}$$

and
$$\boldsymbol{J}_{CL} = \frac{\partial(x,y,z)}{\partial(\bar{x},\bar{y},\bar{z})} = \begin{pmatrix} e_x & -e_y & 0 \\ e_y & e_x & 0 \\ 0 & 0 & 1 \end{pmatrix},$$

where a prime denotes the derivative of a function with respect to its argument, $e_x = \boldsymbol{e}\cdot\boldsymbol{e}_x$ and $e_y = \boldsymbol{e}\cdot\boldsymbol{e}_y$.

The jacobian of the Poincaré map M_{PP} is

$$\boldsymbol{J}_{PP} = \frac{\partial(\hat{\psi},\hat{\zeta},\hat{\tau})}{\partial(\psi,\zeta,\tau)} = \begin{pmatrix} 1+\hat{q}'\Delta' & q'+\hat{q}'(1+q'\Delta') & 0 \\ \Delta' & 1+q'\Delta' & 0 \\ T' & q'T' & 1 \end{pmatrix}$$

(with $\hat{q} \equiv q(\hat{\zeta},\hat{\boldsymbol{e}})$, etc.). This jacobian transports vectors from section to section. Since

a vector can be thought of as joining two close particles carried in the flow, the difference in time and position when they intersect a section give the vector components in a certain basis. Formally, at any point $(x, y, z) = M_{CL} \circ M_{LP}^{(t)}(\psi, \zeta, \tau, \boldsymbol{n}, \boldsymbol{e})$ in an S-region, we can change basis by defining:

$$\begin{aligned}(B_\psi, B_\zeta, B_\tau) &= \partial(\psi, \zeta, \tau)/\partial(x, y, z) \cdot (B_x, B_y, B_z) \\ &= (\boldsymbol{J}_{LP}^{(t)})^{-1} \cdot (\boldsymbol{J}_{CL})^{-1} \cdot (B_x, B_y, B_z). \end{aligned} \tag{14}$$

With this choice of basis at each point the Cauchy solution (13) becomes

$$(B_\psi, B_\zeta, B_\tau)(\boldsymbol{x}, t) = (\boldsymbol{J}_{PP})^n \cdot (B_\psi, B_\zeta, B_\tau)(\boldsymbol{x}_0, 0).$$

These components are simply multiplied by the jacobian $\boldsymbol{J}_{PP}$ as the vector is carried from section to section by the flow. The meaning of the components is evident in the case when $\boldsymbol{x}$ lies on a section $P(\boldsymbol{n}, \boldsymbol{e}_x)$. Then $\boldsymbol{B} = B_\psi \boldsymbol{e}_\psi + B_\zeta \boldsymbol{e}_\zeta + B_\tau \boldsymbol{e}_\tau$, where $\boldsymbol{e}_\psi = \boldsymbol{e}_y$, $\boldsymbol{e}_\zeta = \boldsymbol{e}_z$ and $\boldsymbol{e}_\tau = -\boldsymbol{e}_x - p\boldsymbol{e}_y = -\boldsymbol{u}$. Thus B_τ is the component of field along streamlines and represents the difference in time between the intersections of the two close particles; B_ψ and B_ζ are transverse components which corresponded to the difference in position between the intersections. At general points these components are given by carrying the field, frozen in the flow, to the section and then resolving along $\boldsymbol{e}_\psi$, $\boldsymbol{e}_\zeta$ and $\boldsymbol{e}_\tau$; similar methods are used in Soward (1990).

Certain features of the jacobian $\boldsymbol{J}_{PP}$ arise because the flow is steady. Under multiplication by $\boldsymbol{J}_{PP}$ the component of field along streamlines, B_τ, is conserved in the absence of transverse field components B_ψ and B_ζ. Generally all three components are present and under the jacobian B_τ field is generated from transverse field, because of shearing in the flow, but not vice versa. The evolution of the transverse components can thus be considered independently of B_τ; these will generally grow exponentially because of chaos in the flow. The component B_τ along streamlines is 'slaved' to these transverse components, and is thus of secondary interest. In our numerical study we concentrate on the transverse components for this reason, and also because it is difficult to calculate space averages of the B_τ component. This is because the term $T' = 1/|\psi_X|$ in $\boldsymbol{J}_{PP}$, which represents the conversion of B_ψ to B_τ, is large when $\psi_X \approx 0$. There is a thin sheet of very strong B_τ field thrown off each row of stagnation points. The flux sheet follows the unstable manifold of the stagnation points and in the sheet the peak B_τ field grows exponentially in time, while its scale decreases exponentially. This makes it difficult to resolve space averages of B_τ accurately. However, since the exponential stretching at the rows of X-points generates only B_τ field and not transverse field, it turns out that it is not necessary to resolve the sheets to measure average transverse fields accurately. Thus although B_τ is slaved to the transverse components, it is badly behaved, and we therefore focus on the transverse components, in particular the vertical field, $B_\zeta = B_z$. Note that this slaving only occurs when there is no diffusion, as one effect of diffusion is to generate transverse field from B_τ field; indeed this process is important in certain laminar fast and 'nearly fast' dynamos (Soward 1987; Gilbert 1988).

5. Numerical results

A code was written to follow the evolution of a magnetic field in the *ABCS* flow using the Cauchy solution (11) for zero magnetic diffusion. We study the magnetic field structure on the Poincaré section $P(0, \boldsymbol{e}_x)$. The flow here is largely in the $\boldsymbol{e}_x$

PHILOSOPHICAL TRANSACTIONS OF THE ROYAL SOCIETY A MATHEMATICAL, PHYSICAL & ENGINEERING SCIENCES

direction and sweeps field through the section. To find the field at a point $\boldsymbol{x}$ on the section at time t, the orbit through this point is followed backwards in time, by inverting (12) if $\boldsymbol{x}_0$ lies in an S-region, or (A 1) otherwise. At the same time the code accumulates the product of jacobians in (13) or (A 2) and finally calculates $\boldsymbol{B}(\boldsymbol{x}, t)$ from $\boldsymbol{B}(\boldsymbol{x}_0, 0)$ by (11). Note that the code uses the analytical calculation of jacobians in §4; so the only numerical errors arise through round-off. The great advantage of using the Cauchy solution is that one need not evolve the full three-dimensional structure of the field, but only follow orbits back from points of interest. Furthermore the flow is steady and so to find the magnetic field at $\boldsymbol{x}$ for several different times, one need only follow a single orbit from $\boldsymbol{x}$.

One check of the correctness of the code is to compare the calculation of the jacobian $\partial \boldsymbol{x}/\partial \boldsymbol{x}_0$ by the code with a finite difference approximation obtained by following nearby trajectories. This test of the compatibility of the motion with the jacobian verifies the analytical calculations of §§3 and 4, as well as their numerical implementation. Another test is to verify Stokes' theorem:

$$\int_{\Sigma} \boldsymbol{B} \cdot \mathrm{d}\boldsymbol{S} = \int_{\partial \Sigma} \boldsymbol{A} \cdot \mathrm{d}\boldsymbol{s}, \tag{15}$$

where Σ is a fixed surface, and $\boldsymbol{A}$ is a vector potential for $\boldsymbol{B}$. In a certain gauge the vector potential is transported in the flow by:

$$\boldsymbol{A}(\boldsymbol{x}, t) = (\partial \boldsymbol{x}_0/\partial \boldsymbol{x})^{\mathrm{T}} \cdot \boldsymbol{A}(\boldsymbol{x}_0, 0)$$

(Roberts 1967). Equation (15) was verified for several surfaces Σ by evolving both $\boldsymbol{A}$ and $\boldsymbol{B}$ in the flow up to moderate times.

Figure 4, plate 1, shows pictures of magnetic field evolution in the $ABCS$ flow. The initial condition is

$$\boldsymbol{B}(\boldsymbol{x}, 0) = (\sin(z\sqrt{2}), -\cos(z\sqrt{2}), 0) \tag{16}$$

and we represent the vertical magnetic field B_z on parts of the section $P(0, \boldsymbol{e}_x)$. Because of the exponential stretching of field in the flow there is a large variation of B_z on the section and so a logarithmic scale is used: the quantity

$$F(B_z) = \operatorname{sign}(B_z) \max(\ln|10B_z|, 0)$$

is plotted linearly on the colour scale, which runs from $-F_{\max}$ (blue) to $F_{\max}$ (red), where $F_{\max} = \max|F(B_z)|$ and the maximum is taken over all points in the picture at a given time. A positive B_z component is shown in red, and negative in blue; weak or zero field is in the centre of the scale, being light blue/green. In figure 4*a–c* the field is shown on $x = \frac{1}{2}\pi$, $|z| < \pi/\sqrt{2}$ and $|\psi| < 0.2$, corresponding to figure 3*a*, at times $t = 20$, 50, and 90. As time progresses the structure of regular islands and chaos visible in figure 3*a* becomes apparent in the magnetic field. The weakest fields lie in the islands within the chaotic web (see orbit (3) of figure 3*a*). Layers of strong, fine-scaled field pile up in the chaotic regions of the web (orbit (2) of figure 3*a*); these fields grow exponentially because of chaotic stretching (albeit fairly weak). Outside the web (orbit (1) of figure 3*a*) bands of field form because of persistent vertical shear. These fields are initially fairly strong (figure 3*a–c*); however, they only grow linearly and eventually become insignificant compared with the field in the chaotic regions.

There is also evidence of constructive folding. At $t = 20$ (figure 4*a*) there is mostly positive field (red) at the top and bottom of the picture, and negative field (blue)

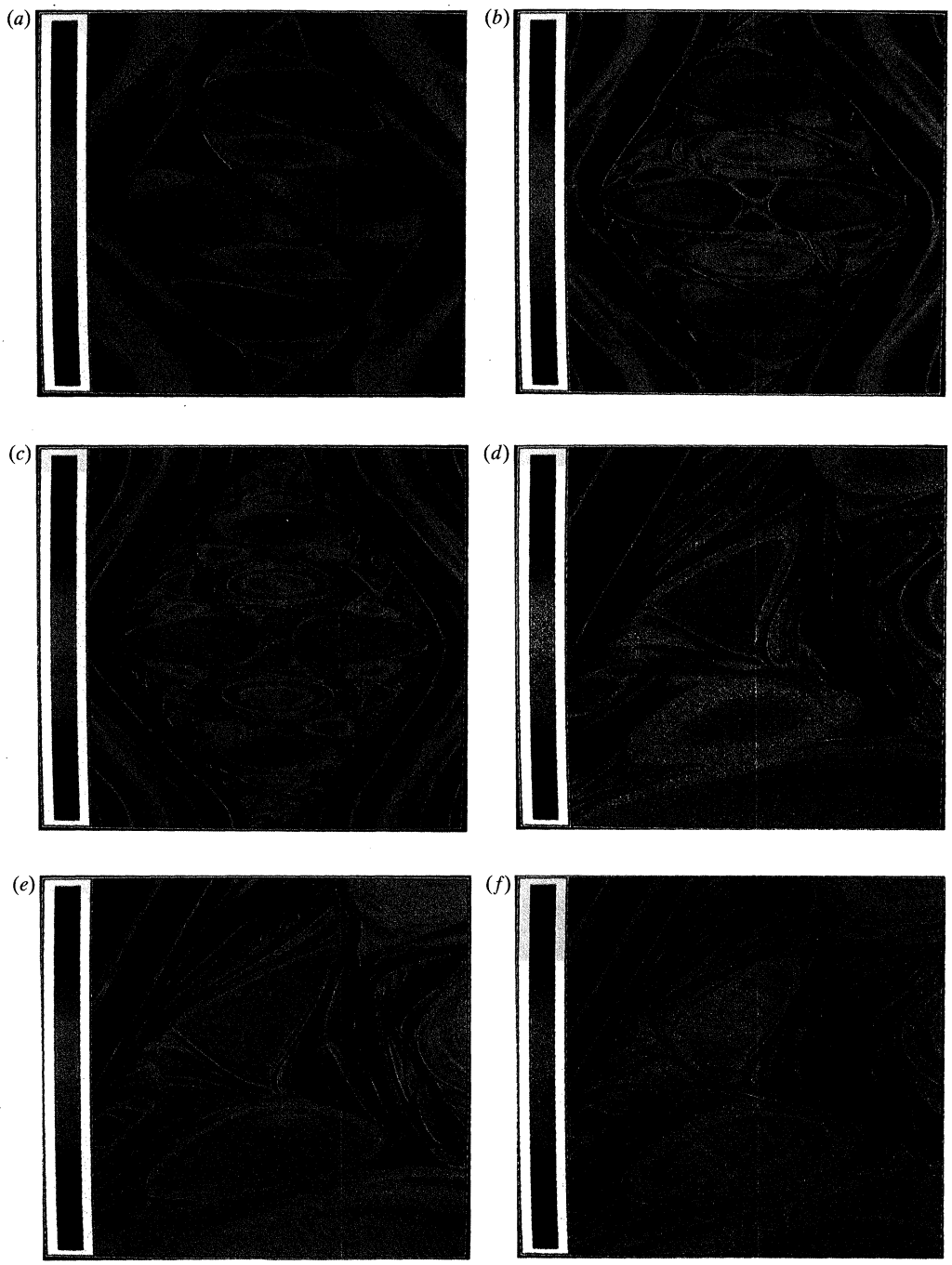

Figure 4. Evolution of magnetic field from the initial condition (16). In (*a–c*) the area of $P(0,\boldsymbol{e}_x)$ shown is that depicted in figure 3*a* while in (*d–f*) it is that in figure 3*b*. The vertical magnetic field B_z is coded as described in the text, with positive B_z shown in red and negative in blue. In (*a*) $t = 20$, (*b*) $t = 50$, (*c*) $t = 90$, (*d*) $t = 90$, (*e*) $t = 130$ and (*f*) $t = 180$.

PHILOSOPHICAL TRANSACTIONS OF THE ROYAL SOCIETY A MATHEMATICAL, PHYSICAL & ENGINEERING SCIENCES

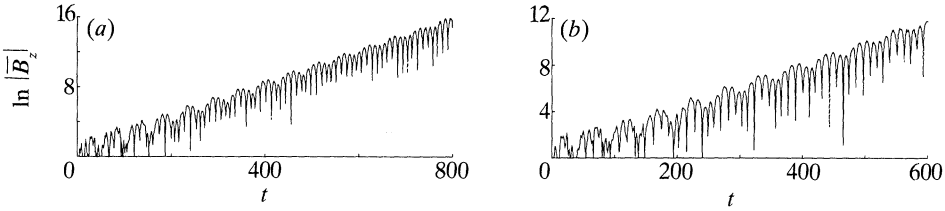

Figure 5. Mean vertical magnetic field $\overline{B_z}$ with the initial condition (16) plotted against time. (*a*) The average is taken over the line A of figure 3*b*; the average over 2^{18} points is shown by the solid line, and over 2^{17} points by the dashed line. (*b*) The average is taken over the line B of figure 3*b*; 2^{16} and 2^{15} points are used for the solid and dashed lines respectively.

mostly in the middle, whereas at $t = 50$ the positive field is mostly in the middle and the negative field at the top and bottom. Note, particularly for $t = 20$, that the field has a distinctive structure of blue or red 'blobs', separated by curved regions of finer scale. The different blobs correspond to streams of fluid that reach the section by different routes through the lattice of X- and S-regions, while the curved regions separating the streams are sheets of fine-scale field stretched along the unstable manifolds of rows of X-points. This is suggestive of a possible dynamo mechanism, namely that constructive folding is achieved by the action of X-points in dividing and recombining streams of fluid (see §7). We have also followed magnetic fields in the real ABC flow (2) with $A = B = 1$ and $C = 0.01$, and observed similar constructive folding.

The structure of the magnetic field at $t = 90$ shown in figure 4*c* is poorly resolved; so figure 4*d–f* show a smaller region of the section, which is that of figure 3*b*, at $t =$ 90, 130 and 180. Again there are fine layers of field piling up in the chaotic regions, and evidence of constructive folding taking place. For example, in the chaotic region seen towards the right of figure 3*b* the field in figure 4*e* is predominantly positive, while in figure 4*f* it is mostly negative.

To quantify the constructive folding we calculate the mean magnetic field component, $\overline{B_z}$, averaged along a line lying in the section and cutting across layers of field. The line taken is that labelled A in figure 3*b*; its precise position is given in the figure caption. Figure 5*a* shows $\ln|\overline{B_z}|$ plotted against time. There are two curves shown; for the solid curve 2^{18} evenly spaced points were used to calculate the average, while for the dashed curve half as many were used. The two curves virtually coincide over the whole range (except near zero crossings of $\overline{B_z}$), showing that the field is well-resolved. There is clear exponential growth of the average field, together with oscillations; between peaks the sign of $\overline{B_z}$ changes, giving characteristic downward spikes in the curve. The period of the oscillations is approximately 21.6; as a comparison, a particle in the chaotic region spends, on average, 4.5 time units between crossing Poincaré sections.

Similar growth and oscillations are obtained when averaging over lines in other chaotic regions for this initial condition. Figure 5*b* shows the growth of $\overline{B_z}$ averaged over line B of figure 3*b*. The growth rate of $\overline{B_z}$ is approximately 0.018; this may be compared with the growth rate of $|\overline{B_z}|$, which is approximately 0.021. These two growth rates are fairly close, indicating that the folding action of the flow is efficient in bringing together like-signed field, and there is relatively little cancellation in calculating the average.

These results have been checked in several ways and appear to be robust. First, the same results are obtained using single precision and double precision arithmetic.

PHILOSOPHICAL TRANSACTIONS OF THE ROYAL SOCIETY A MATHEMATICAL, PHYSICAL & ENGINEERING SCIENCES

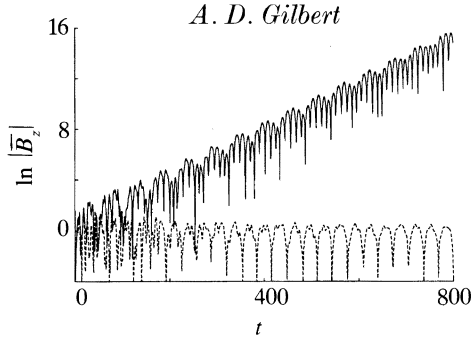

Figure 6. Mean vertical magnetic field $\overline{B_z}$ with the initial condition (16) plotted against time. For the solid line the average is taken over 250^2 points lying in the area marked D in figure 3*b*. For the dashed line the average is taken over 100^2 points lying in the area E of figure 3*b*.

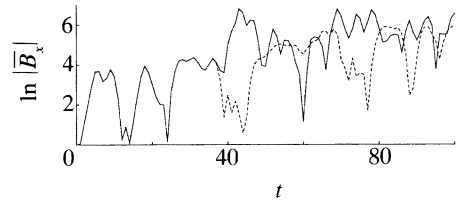

Figure 7. Mean x-directed magnetic field $\overline{B_x}$ with the initial condition (16) plotted against time. The average is taken over the line A of figure 3*b*; the average over 2^{18} points is shown by the solid line, and over 2^{17} points by the dashed line.

Secondly, the growth and oscillations obtained are independent of the precise location of the line within a chaotic region; so the growth observed is not a result of 'edge-effects'. Line segments of shorter lengths were also used; these give similar behaviour, although after a longer transient. Furthermore similar results are found when averaging over areas in the section; the solid line in figure 6 shows the average field over the box D of figure 3*b*, and agrees in detail with figure 5*a* in which the average is taken over the nearby line A. The dashed line in figure 6 shows the average over the box marked E in figure 3*b* and lies in an integrable region. There is a steady decay of field here. Note that since the flow sweeps field across the section, averaging B_z over an area and then over an interval of time corresponds to averaging B_z over a volume in the flow. Thus our results imply that the average magnetic field in a fixed volume in the flow is growing exponentially in time and oscillating; this gives clear evidence of constructive folding in the *ABCS* flow.

Note that averaging over lines is natural in a steady chaotic three-dimensional flow because locally there is a contracting direction, an expanding direction and a neutral direction (along streamlines). A field will develop fine structure only in the contracting direction and it is here that the bulk of the cancellation of flux will occur. In the other two directions the variation of field is relatively weak and so there is little further cancellation. Thus taking averages over lines cutting across the fine structure in the magnetic field seems sufficient to indicate growth of field averaged over areas and volumes.

In §4 we argued that the component of field along streamlines $B_\tau = -B_x$ is more difficult to resolve numerically than the transverse components $B_\psi = -pB_x + B_y$ and $B_\zeta = B_z$. This is confirmed in figure 7, which is similar to figure 5*a*, except that the average x-directed field $\overline{B_x}$ is plotted. This field component is resolved accurately only up to $t \approx 35$.

PHILOSOPHICAL TRANSACTIONS OF THE ROYAL SOCIETY A MATHEMATICAL, PHYSICAL & ENGINEERING SCIENCES

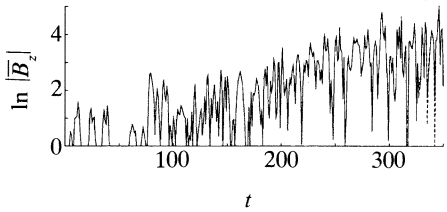

Figure 8. Mean vertical magnetic field $\overline{B}_z$, with the initial condition (17), plotted against time. The average is taken over the line A of figure 3*b*; the average over 2^{18} points is shown by the solid line, and over 2^{17} points by the dashed line.

6. Symmetries of the *ABCS* flow

Not all initial conditions lead to the same clean growth as that seen in figure 5*a* for (16). Figure 8 shows the growth of the average field on the line segment A of figure 3*b* for the superficially similar initial condition

$$\boldsymbol{B}(\boldsymbol{x},0) = (\cos(z\sqrt{2}), \sin(z\sqrt{2}), 0). \tag{17}$$

However, in contrast to figure 5*a* there is very weak growth and it is only possible to follow $\overline{B}_z$ accurately up to $t \approx 300$ using 2^{18} points in the average. These two observations are connected, because the weaker the growth, the more cancellation in calculating the average, and the greater the number of points required to compute the average at a given time. The weak or non-existent growth for this initial condition does not, of course, invalidate our evidence for fast dynamo action in the *ABCS* flow: the induction equation is linear and the growth of a general initial field will soon be dominated by fast-growing fields such as that shown in figure 5*a*. However, the discrepancy between figure 5*a* and figure 8 requires some discussion.

A key to understanding the results of our numerical simulations comes from an examination of the symmetries of the *ABCS* flow. If the magnetic diffusion is non-zero, eigenfunctions and eigenvalues of the induction equation can be classified according to their symmetry properties (Arnold & Korkina 1983; Arnold 1984). In the absence of diffusion eigenfunctions can only exist in some weak, distributional sense (Bayly & Childress 1989; Finn & Ott 1990; Childress & Klapper 1991). However, magnetic fields can still be classified depending on how they transform under the symmetry group, and generally fields of different symmetry have unequal growth rates. This appears to be the explanation for the difference in growth rates between figure 5*a* and 8.

The flow is periodic in space and we shall always identify points modulo the vectors $(\pi,\pi,0)$, $(\pi,-\pi,0)$ and $(0,0,\sqrt{2}\pi)$; so that the flow and field lie on a 3-torus and we can abbreviate $P(\boldsymbol{n},\boldsymbol{e})$ as $P(\boldsymbol{e})$. Having made this identification, the symmetries of the flow form a group isomorphic to the symmetry group of the square. The group has generators r and s satisfying $r^4 = s^2 = i$ and $srs = r^3$, with

$$r(\boldsymbol{x}) = (\pi - y, x, z - \pi/2\sqrt{2}), \quad s(\boldsymbol{x}) = (x, -y, -z).$$

The symmetry r is a rotation of a quarter-turn about the axis $x = y = \frac{1}{2}\pi$ and a translation by a quarter-period in the z direction. The symmetry s is a half rotation about the axis $y = z = 0$, which rotates the Poincaré section $P(\boldsymbol{e}_x)$ of figure 3*a* about its centre. The *ABC* flow (3) possesses the same symmetries. Note that if in addition one allows a transformation to reverse the direction of time, there are further

Table 1. *Character table for the symmetry group of the ABCS flow*

$\chi(g)$	$\{i\}$	$\{r^2\}$	$\{r, r^3\}$	$\{s, r^2s\}$	$\{rs, r^3s\}$
I	1	1	1	1	1
II	1	1	1	−1	−1
III	1	1	−1	1	−1
IV	1	1	−1	−1	1
V	2	−2	0	0	0

symmetries of the flow such as the reflectional symmetries visible in figure 3*a* (Dombre *et al.* 1986). These, however, are not relevant to our study, which involves an initial-value problem.

An element g of the symmetry group also transforms a magnetic field $\boldsymbol{B}$ (taken to have the same periodicity as the flow) to give a field $g[\boldsymbol{B}]$, using the Cauchy solution (11); the generators act as follows:

$$(r[\boldsymbol{B}])(\boldsymbol{x}) = (-B_y, B_x, B_z)(r^{-1}\boldsymbol{x}),$$
$$(s[\boldsymbol{B}])(\boldsymbol{x}) = (B_x, -B_y, -B_z)(s^{-1}\boldsymbol{x}).$$

Given a general magnetic field, the action of the group generates eight linearly independent fields spanning a vector space L. Fields in L are mapped into each other under the group action, and this gives the regular representation of the group. Within this eight dimensional vector space there are minimal subspaces left invariant by the group; these form irreducible representations of the group and give different symmetry classes of magnetic fields (for background see, for example, Hamermesh 1962). The group has five representations, which we label I to V; there are four one-dimensional representations I–IV and one two-dimensional representation V. The one-dimensional representations occur once in the vector space L. The fields

$$\boldsymbol{B}^{\mathrm{I}} = \boldsymbol{B}+r[\boldsymbol{B}]+r^2[\boldsymbol{B}]+r^3[\boldsymbol{B}]+s[\boldsymbol{B}]+rs[\boldsymbol{B}]+r^2s[\boldsymbol{B}]+r^3s[\boldsymbol{B}],$$
$$\boldsymbol{B}^{\mathrm{II}} = \boldsymbol{B}+r[\boldsymbol{B}]+r^2[\boldsymbol{B}]+r^3[\boldsymbol{B}]-s[\boldsymbol{B}]-rs[\boldsymbol{B}]-r^2s[\boldsymbol{B}]-r^3s[\boldsymbol{B}],$$
$$\boldsymbol{B}^{\mathrm{III}} = \boldsymbol{B}-r[\boldsymbol{B}]+r^2[\boldsymbol{B}]-r^3[\boldsymbol{B}]+s[\boldsymbol{B}]-rs[\boldsymbol{B}]+r^2s[\boldsymbol{B}]-r^3s[\boldsymbol{B}],$$
$$\boldsymbol{B}^{\mathrm{IV}} = \boldsymbol{B}-r[\boldsymbol{B}]+r^2[\boldsymbol{B}]-r^3[\boldsymbol{B}]-s[\boldsymbol{B}]+rs[\boldsymbol{B}]-r^2s[\boldsymbol{B}]+r^3s[\boldsymbol{B}],$$

are simply multiplied by a factor $\chi(g)$ when a group element g is applied to them; the values of $\chi(g)$ for different g and representations are given in the character table 1 (Hamermesh 1962). For example, the fields $\boldsymbol{B}^{\mathrm{I}}$ and $\boldsymbol{B}^{\mathrm{III}}$ are even under s, while $\boldsymbol{B}^{\mathrm{II}}$ and $\boldsymbol{B}^{\mathrm{IV}}$ are odd. We postpone discussion of the two-dimensional representation V until §7.

Now the reason for the different growth rates seen in figures 5*a* and 8 becomes clearer. The initial field (16) of figure 5*a* belongs to representation IV, while the initial field (17) of figure 8 is in representation III. Examples of initial fields from representations I and II are

$$\boldsymbol{B}(\boldsymbol{x}, 0) = (\cos(z\sqrt{2}), -\sin(z\sqrt{2}), 0) \tag{18}$$

and

$$\boldsymbol{B}(\boldsymbol{x}, 0) = (\sin(z\sqrt{2}), \cos(z\sqrt{2}), 0) \tag{19}$$

respectively; the growth in $\overline{B_z}$ along the line A of figure 3*b* for these two initial conditions is shown in figure 9. For the initial field (18) there is very weak growth,

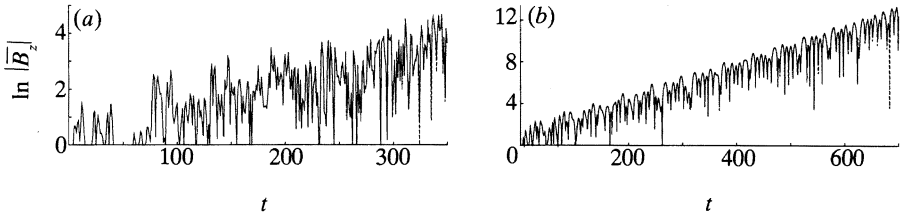

Figure 9. Mean vertical magnetic field $\overline{B_z}$, with the average taken over line A of figure 3*b*, plotted against time; an average over 2^{18} points is shown by the solid lines, and over 2^{17} points by the dashed lines. The initial condition is given by (18) in (*a*) and (19) in (*b*).

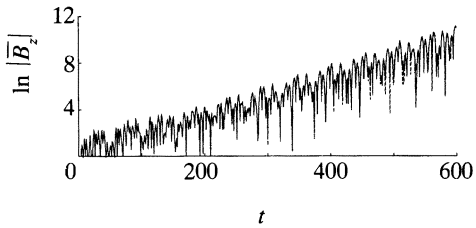

Figure 10. Mean vertical magnetic field $\overline{B_z}$, with the average taken over line A of figure 3*b*, plotted against time; an average over 2^{18} points is shown by the solid lines, and over 2^{17} points by the dashed lines. The initial condition is given by (20).

which is difficult to resolve (figure 9*a*), while for (19) there is well-resolved growth with oscillations (figure 9*b*). We studied several initial conditions belonging to each representation and always find clear growth for fields from representations II and IV, which are odd under the rotation s, with growth rates of 0.016 ± 0.001 and 0.018 ± 0.001 respectively. For representations I and III, which are even under s, we consistently obtain noisy behaviour and weak or no growth.

What is perhaps surprising is that although the growth rates appear to be approximately the same for different fields of the same representation, the frequencies of oscillation can be different. As an example figure 10 shows the growth from the initial condition

$$\boldsymbol{B}(\boldsymbol{x}, 0) = (\cos x \sin y, -\sin x \cos y, 0) \tag{20}$$

which belongs to representation IV. There is growth with oscillations; whereas the growth rate is approximately the same as that for the initial field (16) (see figure 5*a*), the oscillations have about three times the frequency. This is somewhat surprising: if the magnetic diffusion is non-zero, an initial condition from a given representation ultimately grows as the most unstable eigenfunction of that representation. However, in the absence of diffusion, when eigenfunctions exist only in a weak sense, if at all, it appears that an evolving field retains some memory of its initial condition. Initial spatial variations are not entirely wiped out and, as the field is amplified in the flow, these are observed as oscillations when the field is swept through a Poincaré section. Indeed the initial field (20) has more variation than (16) along streamlines, as may be verified by plotting $B_z(\boldsymbol{x}(t))$ as a function of time for a chaotic streamline, $\boldsymbol{x}(t)$. Note that a similar situation occurs in the two idealized dynamo models to be introduced in §7 and those discussed by Finn *et al.* (1991, §3), in which fields with different spatial periodicities have the same growth rate. This degenerate situation would be changed by weak diffusion, which would tend to reduce the growth of fields with more spatial variation and thus lead to a loss of memory of the initial condition.

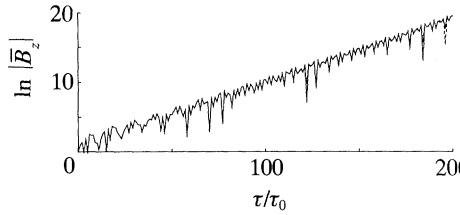

Figure 11. Mean vertical magnetic field $\overline{B_z}$, with the average taken over line A of figure 3*b*, plotted against number of iterations, τ/τ_0; an average over 2^{15} points is shown by the solid lines, and over 2^{14} points by the dashed lines. The initial condition is given by (16).

Our results suggest that in the limit of weak diffusivity η there may be a number of eigenvalues whose real parts tend to a single positive fast dynamo growth rate, but which possess distinct imaginary parts corresponding to differing degrees of spatial structure. This seems to correspond to the condensation of eigenvalues discussed by Vishik (1989, §2).

7. Dynamo mechanisms

We have seen constructive folding and the exponential growth of averaged field in the *ABCS* flow, suggesting fast dynamo action. In this section we discuss the dynamo mechanism and how one might model it. The discussion is somewhat tentative in view of the complexity of the *ABCS* flow, and in the absence of any kind of detailed theory. The mechanism is related to the stretch–fold–shear dynamo (Bayly & Childress 1988, 1989; Finn *et al.* 1991); we have not identified any stretch–twist–fold mechanisms (Vainshtein & Zeldovich 1972) in the flow.

First consider the action of the rows of hyperbolic, X-type, stagnation points in the flow. Two distinct effects may be identified. The first 'cut and paste' effect is that the two streams of fluid impinging on an X-point are divided and recombined into two streams which part in opposite directions. Thus two particles, initially close together, can be separated by an X-point, and take different paths through the lattice; this effect may be seen in figure 4. The second 'shear' effect is that fluid elements are sheared out along streamlines, since particles which pass close to an X-point are delayed for long periods of time. Thus particles which take the same path through the network of S- and X-regions are separated by this process. Because of the shearing strong B_τ components of field are generated very close to X-points; however, these are decoupled and can be ignored, as discussed in §4.

To understand the rôle of these two effects we study magnetic field evolution in a modified flow, for which the shear effect is absent and the only effect of the X-points is the cutting and pasting of streams of fluid. Call this the *ABCS* 1 model for brevity. Suppose that every fluid element traverses an X-region in a fixed time τ_0, while undergoing the same vertical displacement as before. Then particles can be followed from section to section by increasing τ by τ_0 and iterating the Poincaré map M_{PP} (10) taking $(\psi, \zeta, \boldsymbol{n}, \boldsymbol{e}) \to (\hat{\psi}, \hat{\zeta}, \hat{\boldsymbol{n}}, \hat{\boldsymbol{e}})$ without further changing τ. At the same time the transverse field components B_ψ and B_ζ are evolved using the appropriate sub-matrix of $\boldsymbol{J}_{PP}$. The modified flow could be constructed explicitly by replacing the flow in an X-region by an accelerated corner flow, as used by Soward (1987). Note that the modified flow is not continuous; each section maps onto two other sections in a finite time τ_0, and so fluid elements are torn apart at the corner. Figure 11 shows the evolution of $\overline{B_z}$, averaged along the line A of figure 3*b* for the initial condition (16),

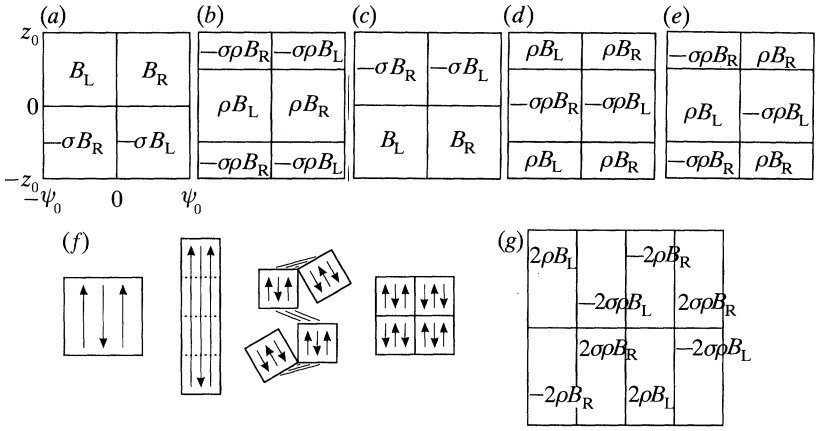

Figure 12. Model stretch–fold–cut–paste dynamo illustrated for a field from one of representations I to IV. (*a*) The section $P^{(0)}(\boldsymbol{e}_x)$ is divided into four quadrants, each with the uniform initial vertical field shown. The initial field on the other sections is given by applying r and multiplying by ρ to give $P^{(0)}(\boldsymbol{e}_y)$ in (*b*), $P^{(0)}(-\boldsymbol{e}_x)$ in (*c*), and $P^{(0)}(-\boldsymbol{e}_y)$ in (*d*). (*e*) In the cut–paste step, the field on the left side ($\psi < 0$) of $P^{(0)}(\boldsymbol{e}_y)$ is carried to the left side of $P^{(\frac{1}{2})}(\boldsymbol{e}_x)$, and the field from the right side of $P^{(0)}(-\boldsymbol{e}_y)$ to the right side of $P^{(\frac{1}{2})}(\boldsymbol{e}_x)$. (f) In the stretch-fold step the baker's map shown schematically is applied to $P^{(\frac{1}{2})}(\boldsymbol{e}_x)$, and similarly for the other sections. (*g*) The resulting field on $P^{(1)}(\boldsymbol{e}_x)$ is shown.

as a function of the number of iterations, τ/τ_0, of M_{PP}. There is clear exponential growth of the average at a rate of about $0.090/\tau_0$. Given that a particle in the chaotic region spends, on average, 4.5 time units travelling between sections, this may be translated crudely into a growth rate of 0.020 per time unit by taking $\tau_0 = 4.5$. This is close to the growth rate of 0.018 observed in the *ABCS* flow for this initial condition, and suggests that the shearing effect of the X-points is relatively unimportant in the dynamo mechanism. The two crucial effects seem to be the chaos in the flow, which gives exponential stretching, and the cutting and pasting at X-points. One could call this a stretch–fold–cut–paste dynamo. The mechanism is broadly similar to the stretch–fold–slide dynamos discussed by Finn *et al.* (1991) and Klapper (1991). Note that the cutting and pasting at the X-points is essential because a continuous map from section to section would fail to be a dynamo (Cowling 1934; Zeldovich 1957).

We now sketch a crude model of a stretch–fold–cut–paste dynamo, called *ABCS* 2, which is based on baker's maps (Finn & Ott 1988). This is intended to illustrate how such a dynamo might operate rather to model the *ABCS* flow in any detail; however, the model and the flow turn out to have a number of features in common. Like the *ABCS* 1 model, the map takes field from section to section; we take the chaotic part of each section to be given by the rectangle, $0 \leqslant |\psi| < \psi_0$ and $|z| < \pi/\sqrt{2} \equiv z_0$. We demand that the *ABCS* 2 map have the same symmetries as the *ABCS* flow and for simplicity take an initial magnetic field $\boldsymbol{B}$ belonging to one of the representations I to IV; so that $s[\boldsymbol{B}] = \sigma\boldsymbol{B}$ and $r[\boldsymbol{B}] = \rho\boldsymbol{B}$ with $\sigma = \pm 1$ and $\rho = \pm 1$. For the initial field, divide the section $P^{(0)}(\boldsymbol{e}_x)$ into four quadrants (figure 12*a*); take the initial field to be uniform and vertical in each quadrant and to be consistent with $s[\boldsymbol{B}] = \sigma\boldsymbol{B}$, as shown in figure 12*a*. Here the superscript in $P^{(0)}(\boldsymbol{e}_x)$ denotes the iteration number. The field on the other sections is obtained by repeatedly applying the symmetry r and multiplying by ρ, as shown in figure 12*b*–*d*.

The model dynamo map comprises two operations, cut–paste and stretch–fold. First model the cutting and pasting action of the row of X-points at the origin. At iteration $m = \frac{1}{2}$, after the cut–paste operation, the field on the left side ($\psi < 0$) of $P^{(\frac{1}{2})}(\boldsymbol{e}_x)$ is that which was on the left side of $P^{(0)}(\boldsymbol{e}_y)$ (figure 12*b*) at iteration $m = 0$, while the field on the right side of $P^{(\frac{1}{2})}(\boldsymbol{e}_x)$ comes from the right side ($\psi > 0$) of $P^{(0)}(-\boldsymbol{e}_y)$ (figure 12*d*). The field resulting after this cut and paste operation is shown in figure 12*e*. Formally let $B_z(\psi, z, \boldsymbol{e}, m)$ denote the vertical field on $P^{(m)}(\boldsymbol{e})$ at iteration m for a field of any symmetry; then the cut–paste operation is given by

$$B_z(\psi, z, \boldsymbol{e}, m+\tfrac{1}{2}) = B_z(\psi, z, (\boldsymbol{e}\times\boldsymbol{e}_z)\,\mathrm{sign}\,(\psi), m).$$

In the second operation we model the stretching and folding by the chaos in the flow. This is most easily achieved using a baker's map, although in the actual flow the stretching is much weaker. The baker's map chosen must be invariant under the symmetries, in particular under s, which rotates the section $P(\boldsymbol{e}_x)$ by π about its centre. The simplest map with this property is shown schematically in figure 12*f*. Applying it to the field in figure 12*e* gives the field at iteration $m = 1$ on $P^{(1)}(\boldsymbol{e}_x)$ shown in figure 12*g*. Formally the baker's map on the section $P(\boldsymbol{e}_x)$ is given by

$$B_z(\psi, z, \boldsymbol{e}_x, m+1) = \begin{cases} 2B_z(\psi_0+2\psi, \tfrac{1}{2}z, \boldsymbol{e}_x, m+\tfrac{1}{2}), & z>0, \psi<0, \\ -2B_z(\psi_0-2\psi, z_0-\tfrac{1}{2}z, \boldsymbol{e}_x, m+\tfrac{1}{2}), & z>0, \psi>0, \\ 2B_z(-\psi_0+2\psi, \tfrac{1}{2}z, \boldsymbol{e}_x, m+\tfrac{1}{2}), & z<0, \psi>0, \\ -2B_z(-\psi_0-2\psi, -z_0-\tfrac{1}{2}z, \boldsymbol{e}_x, m+\tfrac{1}{2}), & z<0, \psi<0. \end{cases}$$

We require that the stretch–fold map commutes with r as well as s, and this determines similar baker's maps that are applied on the other sections.

Define F_{L} and F_{R} as the net vertical fluxes in the top left and top right quadrants of the field in figure 12*a*, then under the mapping $F_{\mathrm{L}} \to \rho(1-\sigma)F_{\mathrm{L}}$ and $F_{\mathrm{R}} \to \rho(\sigma-1)F_{\mathrm{R}}$. As the map is iterated the fluxes F_{L} and F_{R} grow exponentially if $\sigma = -1$, because of constructive folding. If $\sigma = 1$ the folding is not constructive and the fluxes become zero after one iteration. Despite the crudeness of the model, this corresponds closely to the *ABCS* flow, where there is growth of field for representations II and IV, which have $\sigma = -1$, and very weak or no growth for representations I and III.

Finally, consider the two-dimensional representation V, which has been postponed up to now since our numerical results are difficult to interpret. This representation occurs twice in the vector space L. Given a general field $\boldsymbol{B}$ define two pairs of fields:

$$\begin{aligned} \boldsymbol{B}_1^{\mathrm{V}1} &= \boldsymbol{B} - r^2[\boldsymbol{B}] + s[\boldsymbol{B}] - r^2 s[\boldsymbol{B}], \\ \boldsymbol{B}_2^{\mathrm{V}1} &= r[\boldsymbol{B}] - r^3[\boldsymbol{B}] + rs[\boldsymbol{B}] - r^3 s[\boldsymbol{B}], \\ \text{and} \qquad \boldsymbol{B}_1^{\mathrm{V}2} &= -r[\boldsymbol{B}] + r^3[\boldsymbol{B}] + rs[\boldsymbol{B}] - r^3 s[\boldsymbol{B}], \\ \boldsymbol{B}_2^{\mathrm{V}2} &= \boldsymbol{B} - r^2[\boldsymbol{B}] - s[\boldsymbol{B}] + r^2 s[\boldsymbol{B}]; \end{aligned}$$

each of these pairs spans a vector space which is invariant under the group action. For each pair the action of an element g is described by a matrix $\boldsymbol{D}(g)$:

$$g[\boldsymbol{B}_l] = \sum_{k=1}^{2} \boldsymbol{B}_k D_{kl}(g).$$

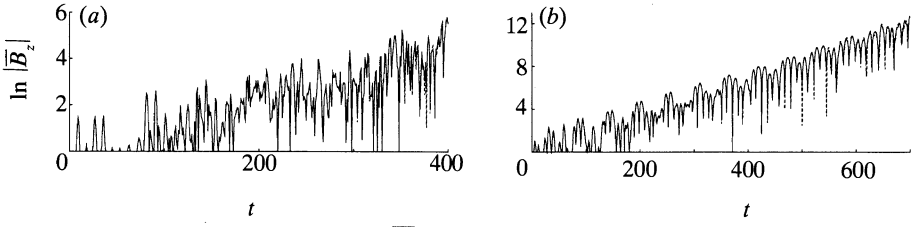

Figure 13. Mean vertical magnetic field $\overline{B_z}$, with the average taken over line A of figure 3*b*, plotted against time; an average over 2^{18} points is shown by the solid lines, and over 2^{17} points by the dashed lines. The initial condition is given by (21) in (*a*) and (22) in (*b*).

The matrices $\boldsymbol{D}(g)$ are given explicitly by

$$\boldsymbol{D}(i)=\begin{pmatrix}1&0\\0&1\end{pmatrix},\quad \boldsymbol{D}(r)=\begin{pmatrix}0&-1\\1&0\end{pmatrix},\quad \boldsymbol{D}(r^2)=\begin{pmatrix}-1&0\\0&-1\end{pmatrix},\quad \boldsymbol{D}(r^3)=\begin{pmatrix}0&1\\-1&0\end{pmatrix},$$

$$\boldsymbol{D}(s)=\begin{pmatrix}1&0\\0&-1\end{pmatrix},\quad \boldsymbol{D}(rs)=\begin{pmatrix}0&1\\1&0\end{pmatrix},\quad \boldsymbol{D}(r^2s)=\begin{pmatrix}-1&0\\0&1\end{pmatrix},\quad \boldsymbol{D}(r^3s)=\begin{pmatrix}0&-1\\-1&0\end{pmatrix}.$$

The characters of the representation given in table 1 are the traces of the matrices.

Before giving numerical results, consider the crude baker's map model (*ABCS* 2) of a stretch–fold–cut–paste dynamo introduced earlier and recall that for representations I to IV, fields that are odd under s grow, while fields that are even show weak or no growth. A field of the form $\boldsymbol{B}_1^{\mathrm{V}}$ has a mixed character; $\boldsymbol{B}_1^{\mathrm{V}}$ is even under s, while $r[\boldsymbol{B}_1^{\mathrm{V}}]=\boldsymbol{B}_2^{\mathrm{V}}$ is odd. In other words the field $\boldsymbol{B}_1^{\mathrm{V}}$ is even under rotation of the section $P(\pm\boldsymbol{e}_x)$ (by s), but odd under similar rotations of $P(\pm\boldsymbol{e}_y)$ (by r^2s). In the context of the *ABCS* 2 model an initial field $\boldsymbol{B}_1^{\mathrm{V}}$ is represented by taking an even field on $P^{(0)}(\pm\boldsymbol{e}_x)$:

$$B_z(\psi,z,\pm\boldsymbol{e}_x,0)=(sB_z)(\psi,z,\pm\boldsymbol{e}_x,0)\equiv -B_z(-\psi,-z,\pm\boldsymbol{e}_x,0),$$

but an odd field on $P^{(0)}(\pm\boldsymbol{e}_y)$:

$$B_z(\psi,z,\pm\boldsymbol{e}_y,0)=-(r^2sB_z)(\psi,z,\pm\boldsymbol{e}_y,0)\equiv B_z(-\psi,-z+z_0,\pm\boldsymbol{e}_y,0).$$

Now note that as the *ABCS* 2 map is iterated, even fields are never mixed with odd fields, i.e. for m even (odd respectively) $B_z(\psi,z,\pm\boldsymbol{e}_x,m)$ is always even (odd) under s, while $B_z(\psi,z,\pm\boldsymbol{e}_y,m)$ is always odd (even) under r^2s. It follows from the previous discussion of the model that the odd fields should show clear growth, while the even fields show no growth.

Something broadly similar appears to happen in the *ABCS* flow. For initial conditions of the form $\boldsymbol{B}_1^{\mathrm{V}}$, there is clear growth of $\overline{B_z}$ when averaged along line B of figure 3*b*, but when averaged along lines A or C there is noisy behaviour, and weak or no growth. For fields of the form $\boldsymbol{B}_2^{\mathrm{V}}$ there is clean growth for lines A and C, but weak or no growth for line B. An example is the pair of initial conditions:

$$\boldsymbol{B}_1^{\mathrm{V}}(\boldsymbol{x},0)=(0,\sin(2z\sqrt{2}),0),\tag{21}$$

$$\boldsymbol{B}_2^{\mathrm{V}}(\boldsymbol{x},0)=(\sin(2z\sqrt{2}),0,0),\tag{22}$$

which are related by a rotation r. Figure 13*a*, *b* shows the growth of $\overline{B_z}$, with the average taken along line A of figure 3*b* for these two initial conditions.

PHILOSOPHICAL TRANSACTIONS OF THE ROYAL SOCIETY A MATHEMATICAL, PHYSICAL & ENGINEERING SCIENCES

We do not have a simple explanation for this somewhat bizarre behaviour. However, the baker's map model and the numerical results suggest that the chaotic web in the *ABCS* flow splits (at least approximately) into two distinct regions related by the symmetry r. In one region, which includes line B of figure 3*b*, $\boldsymbol{B}_1^{\mathrm{V}}$ fields are amplified strongly, but not $\boldsymbol{B}_2^{\mathrm{V}}$ fields; in the other region, which includes lines A and C, $\boldsymbol{B}_2^{\mathrm{V}}$ fields are amplified strongly and not $\boldsymbol{B}_1^{\mathrm{V}}$ fields. If weak magnetic diffusion is introduced, the dynamo eigenfunctions belonging to representation V can again be split up into pairs $\boldsymbol{B}_1^{\mathrm{V}}$ and $\boldsymbol{B}_2^{\mathrm{V}}$. Our numerical results suggest that these may be localized only in certain regions of the chaotic web.

8. Numerical methods for *ABC* flows

We now return to the *ABC* flows (2) and seek evidence for constructive folding and fast dynamo action. To find the field at a point $\boldsymbol{x}_1$ at time T, follow the motion of a particle backwards in time from this point; letting $\alpha = T - t$, integrate $\boldsymbol{x}(\alpha)$ by

$$\partial_\alpha \boldsymbol{x} = -\boldsymbol{u}(\boldsymbol{x}), \quad \boldsymbol{x}(0) = \boldsymbol{x}_1$$

from $\alpha = 0$ to $\alpha = T$ to obtain $\boldsymbol{x}_0 = \boldsymbol{x}(T)$. Also define the jacobian

$$J_{ij}(\alpha) = \partial x_i(0)/\partial x_j(\alpha)$$

and integrate it according to

$$\partial_\alpha J_{ij} = J_{ik} S_{jk}, \quad J_{ij}(0) = \delta_{ij},$$

where $S_{ki}(\alpha) \equiv \partial_k u_i(\boldsymbol{x}(\alpha))$. The Cauchy solution is then

$$B_i(\boldsymbol{x}_1, t = T) = J_{ij}(T) B_j(\boldsymbol{x}_0, t = 0).$$

An alternative method is to exploit the fact that the flow is steady and resolve field parallel and transverse to streamlines; this leads to some simplifications as for the *ABCS* flow. Given a vector field $\boldsymbol{a}(\alpha) \equiv \boldsymbol{a}(\boldsymbol{x}(\alpha))$ defined along the streamline $\boldsymbol{x}(\alpha)$, define

$$\mathscr{L}\boldsymbol{a} = \partial_\alpha \boldsymbol{a} + \boldsymbol{a} \cdot \boldsymbol{S}.$$

If the vector field is generated by carrying a vector frozen in the fluid along the streamline, then $\mathscr{L}\boldsymbol{a} = 0$. An example is the flow itself, which satisfies $\mathscr{L}\boldsymbol{u} = 0$. To find the field at a point $\boldsymbol{x}_1$ at time T, begin by defining a right-handed orthogonal basis $\{\boldsymbol{u}_1, \boldsymbol{v}_1, \boldsymbol{w}_1\}$ at this point with $\boldsymbol{u}_1 = \boldsymbol{u}(\boldsymbol{x}_1)$, and set $\boldsymbol{v}(\boldsymbol{x}_1) = \boldsymbol{v}_1$ and $\boldsymbol{w}(\boldsymbol{x}_1) = \boldsymbol{w}_1$. Suppose we freeze $\boldsymbol{v}$ and $\boldsymbol{w}$ in the flow, setting $\mathscr{L}\boldsymbol{v} = \mathscr{L}\boldsymbol{w} = 0$ along the streamline. The components of field in the basis $\{\boldsymbol{u}, \boldsymbol{v}, \boldsymbol{w}\}$ are then conserved when a frozen field vector is carried along the streamline. Thus the components of the final field are given simply by resolving the initial field onto the basis $\{\boldsymbol{u}, \boldsymbol{v}, \boldsymbol{w}\}$ at the point $\boldsymbol{x}_0$. This method, however, is not ideal, since as the basis is carried in the flow, the angles between the basis vectors decrease exponentially, and at $\boldsymbol{x}_0$, there will be large errors in calculating the components of the initial field in the basis. It is more convenient to carry the vectors along the streamline in such a way as to keep the basis orthogonal, and so we define $\boldsymbol{v}_\perp$ and $\boldsymbol{w}_\perp$ by

$$\boldsymbol{v} = \boldsymbol{v}_\perp + \lambda \boldsymbol{u}, \quad \boldsymbol{w} = \boldsymbol{w}_\perp + \mu \boldsymbol{u} + \nu \boldsymbol{v}_\perp$$

with $\boldsymbol{u}\cdot\boldsymbol{v}_\perp = \boldsymbol{u}\cdot\boldsymbol{w}_\perp = \boldsymbol{v}_\perp\cdot\boldsymbol{w}_\perp = 0$. The vectors $\boldsymbol{v}_\perp$ and $\boldsymbol{w}_\perp$ and the scalars λ, μ and ν evolve along the streamline according to:

$$\left.\begin{aligned} &\mathscr{L}\boldsymbol{v}_\perp = -\boldsymbol{u}\,\partial_\alpha\lambda, \quad \mathscr{L}\boldsymbol{w}_\perp = -\boldsymbol{u}(\partial_\alpha\mu - \nu\,\partial_\alpha\lambda) - \boldsymbol{v}_\perp\,\partial_\alpha\nu,\\ &\partial_\alpha\lambda = -\boldsymbol{u}\cdot(\boldsymbol{S}+\boldsymbol{S}^T)\cdot\boldsymbol{v}_\perp/u^2, \quad \partial_\alpha\mu - \nu\,\partial_\alpha\lambda = -\boldsymbol{u}\cdot(\boldsymbol{S}+\boldsymbol{S}^T)\cdot\boldsymbol{w}_\perp/u^2,\\ &\partial_\alpha\nu = -\boldsymbol{v}_\perp\cdot(\boldsymbol{S}+\boldsymbol{S}^T)\cdot\boldsymbol{w}_\perp/v_\perp^2. \end{aligned}\right\} \tag{23}$$

At $\alpha = 0$ set $\boldsymbol{v}_\perp = \boldsymbol{v}_1$, $\boldsymbol{w}_\perp = \boldsymbol{w}_1$ and $\lambda = \mu = \nu = 0$. At $\alpha = T$ when $\boldsymbol{x} = \boldsymbol{x}_0$, resolve the initial field onto the basis by writing $\boldsymbol{B}_0 = B_u\,\boldsymbol{u} + B_v\,\boldsymbol{v}_\perp + B_w\,\boldsymbol{w}_\perp$. The result of carrying this vector in the flow to $\boldsymbol{x}_1$ is

$$\boldsymbol{B}_1 = (B_u - \lambda B_v - (\mu - \nu\lambda)\,B_w)\,\boldsymbol{u}_1 + (B_v - \nu B_w)\,\boldsymbol{v}_1 + B_w\,\boldsymbol{w}_1. \tag{24}$$

There is some redundancy in this method; $\boldsymbol{u}\cdot\boldsymbol{v}_\perp\times\boldsymbol{w}_\perp = V_0$ is constant along a streamline, as the flow is volume preserving and so $\boldsymbol{w}_\perp$ may be eliminated by writing $\boldsymbol{w}_\perp = (\boldsymbol{u}\times\boldsymbol{v}_\perp)(V_0/u^2v_\perp^2)$. Furthermore, as in the *ABCS* flow, the field component B_u along streamlines is slaved to the transverse components B_v, B_w. Thus we shall focus solely on the transverse components, and so need only integrate the equations for $\boldsymbol{v}_\perp$ and ν back along a streamline.

9. Results for the *ABC* flow with $A = B = C = 1$

In this section we study magnetic field evolution in the *ABC* flow with $A = B = C = 1$, which possesses the symmetries listed in Appendix B. The flow also has a network of stagnation points joined by separatrices, as discussed by Childress & Soward (1985). Consider a Poincaré section in the flow that intersects the separatrix joining the stagnation points at $(-\frac{1}{4}\pi)(1,1,1)$ and $(\frac{3}{4}\pi)(1,1,1)$. Define coordinates $(\tilde{x},\tilde{y},\tilde{z})$ by

$$\begin{aligned} \boldsymbol{x} &= \boldsymbol{c} + \tilde{x}\boldsymbol{e}_{\tilde{x}} + \tilde{y}\boldsymbol{e}_{\tilde{y}} + \tilde{z}\boldsymbol{e}_{\tilde{z}}\\ &\equiv (\tfrac{1}{4}\pi)(1,1,1) + (\tilde{x}/\sqrt{2})(-1,1,0) + (\tilde{y}/\sqrt{6})(-1,-1,2) + (\tilde{z}/\sqrt{3})(1,1,1); \end{aligned} \tag{25}$$

so that the section is given by $\tilde{z} = 0$. Figure 14 shows part of the section given by $|\tilde{x}| < 0.15$ and $|\tilde{y}| < 0.15$; the separatrix intersects the section at its centre $\tilde{x} = \tilde{y} = 0$ and the flow has three-fold symmetry about this point.

The second method of §8 is used to evolve field in the flow. At each point on the section define a vector radial to the separatrix, $\boldsymbol{v} = \tilde{x}\boldsymbol{e}_{\tilde{x}} + \tilde{y}\boldsymbol{e}_{\tilde{y}}$; project this vector perpendicular to $\boldsymbol{u}_1$ and normalize it to unit length to obtain $\boldsymbol{v}_1$. This vector is approximately radial to the separatrix, as the flow is mostly in the $\boldsymbol{e}_{\tilde{z}}$ direction. Now integrate $\boldsymbol{v}_\perp$ and ν back along streamlines using (23) and then calculate the final transverse field from (24). The initial field giving the clearest evidence for constructive folding in the flow is

$$\boldsymbol{B}(\boldsymbol{x},0) = (\sin z - \cos y, \sin x - \cos z, \sin y - \cos x), \tag{26}$$

which belongs to the one-dimensional representation labelled II in Appendix B. Pictures giving graphical evidence for constructive folding of the B_v component field are presented in Gilbert (1991). To confirm this we calculate the average radial field component $\overline{B_v}$ along the line marked A in figure 14; this quantity is plotted in figure 15*a* and there is clear exponential growth with oscillations (Gilbert 1991). The

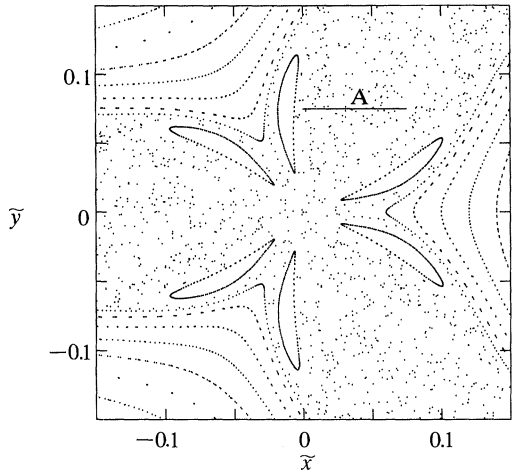

Figure 14. Poincaré section of the ABC flow with $A = B = C = 1$, given by $|\tilde{x}| < 0.15$ and $|\tilde{y}| < 0.15$ The line A is given by $0 < \tilde{x} < 0.075$, $\tilde{y} = 0.075$.

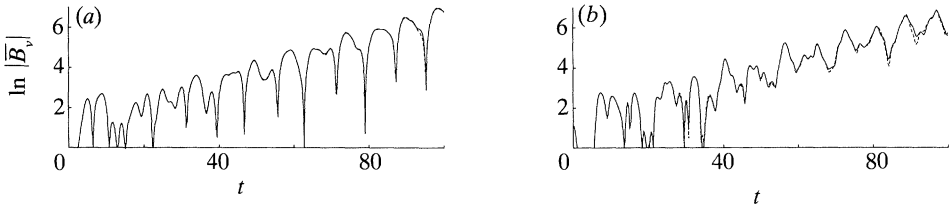

Figure 15. Mean magnetic field $\overline{B_v}$ averaged over line A of figure 14 plotted against time. The initial conditions are (*a*) equation (26) and (*b*) equation (27).

growth rate here is approximately 0.05. It was not possible to follow this growth for very long periods of time, partly because of the expense of integrating back along streamlines with sufficient accuracy, and partly because of the difficulty of resolving fine enough scales to obtain the average $\overline{B_v}$; the reason is that the fine sheets of field thrown off the three-dimensional hyperbolic stagnation points contain strong transverse field and it is necessary to resolve these. This resolution problem was absent in the $ABCS$ flow, because the stagnation points are essentially two-dimensional, lying in degenerate rows, and so do not generate strong transverse fields. For the solid line in figure 15*a* 14000 points spaced unequally (and down to as little as 10^{-8} apart) along the line were used to calculate the average, while for the dashed line 4000 points were used. There is thus again clear evidence of constructive folding. As in the $ABCS$ model the field along streamlines is much stronger than the transverse field, although slaved to the transverse field.

Several initial conditions for each of the five representations of the symmetry group (see Appendix B) were used. Representation I gives only noisy behaviour and weak or no growth, but for the remaining representations initial conditions were found giving clear growth. An example for representation III is

$$\boldsymbol{B}(\boldsymbol{x}, 0) = (2\sin z + 2\cos y, -\sin x - \cos z, -\sin y - \cos x), \tag{27}$$

and the growth in $\overline{B_v}$ is shown in figure 15*b*. All the growth rates observed are approximately the same, around 0.04 and 0.05. We considered several initial fields from each representation and found evidence that different initial fields belonging to

the same representation may have similar growth rates but different frequencies of oscillation, as for the *ABCS* flow. However, because of the difficulty in resolving the average fields accurately over long times, we were unable to conduct a very complete survey.

It is interesting to compare these results with the results of Arnold & Korkina (1983) and Galloway & Frisch (1986). In the first window of dynamo action $9 \lesssim R_m \lesssim 17.5$, the fastest growing eigenmode belongs to the representation II, while in the second window the eigenmode belongs to representation V and at $R_m = 550$ has a growth rate of about 0.08. Thus our growth rates are comparable to those observed in Galloway & Frisch (1986) although somewhat smaller, and our calculations suggest that at sufficiently high magnetic Reynolds numbers, eigenmodes belonging to representations II to V should be unstable. Possible discrepancies between our results and numerical calculations at large finite R_m (D. J. Galloway, personal communication) may be because R_m is not sufficiently large. This problem is particularly acute for the $A = B = C = 1$ case since the chaotic regions occupy only a small volume of space; large values of R_m and correspondingly fine numerical grids (Moffatt & Proctor 1985) are necessary to allow the field to develop structure within chaotic regions.

10. Discussion

We have approached the fast dynamo problem by studying the evolution of magnetic field in steady chaotic flows for the case of zero magnetic diffusion. This approach has the advantage that the Cauchy solution may be used to follow magnetic field vectors and so the evolution of field in small regions of the flow may be studied without employing a fine three-dimensional grid. Two flows were studied, an *ABC* flow and a model flow, the *ABCS* flow, which is constructed by patching together simple flows. The action of the chaos in each flow is to stretch and fold magnetic field, generating fine-scale structure. However, for both flows constructive folding is observed: there is exponential growth of magnetic field averaged over parts of the chaotic web, implying that there is persistent structure in the growing field on the scale of the web. The evidence for this is particularly clear for the *ABCS* flow, which is designed to allow field to be followed inexpensively over long periods of time. Since the principal effect of weak diffusion is to smooth field locally, the constructive folding seen is suggestive of fast dynamo action in these flows. This is still a tentative conclusion as no rigorous results are known about the relation between the case of zero magnetic diffusion and the fast dynamo problem for flows of any complexity. However, a connection can be made in certain idealized models; for the stretch–fold–shear model (Bayly & Childress 1989; Finn *et al.* 1991) and certain hyperbolic maps (Klapper 1992*b*) exponential growth in averaged field at zero magnetic diffusion does imply fast dynamo action.

The *ABC* and *ABCS* flows possess symmetries, and magnetic fields belonging to different representations of the appropriate symmetry group generally have different growth rates. Several initial conditions belonging to each representation were studied; these appear to have the same growth rate, but may have different frequencies of oscillation, depending on the degree of spatial structure in the initial condition. This degeneracy would presumably be removed if weak diffusion were introduced. Initial conditions belonging to the two-dimensional representation showed growth in some regions of the chaotic web and not in others, suggesting that with diffusion the corresponding eigenfunctions may be localized only in certain

PHILOSOPHICAL TRANSACTIONS OF THE ROYAL SOCIETY A MATHEMATICAL, PHYSICAL & ENGINEERING SCIENCES

parts of the web. Possible dynamo mechanisms for the *ABCS* flow were studied. It appears that the cutting and pasting of streams of fluid at the rows of X-points is important in allowing field to be folded constructively in the web. An illustrative model of a dynamo based on this process, together with stretching and folding, was introduced; the model reproduces some qualitative features of dynamo action in the *ABCS* flow.

Certain qualitative effects are absent from our simulations because we have taken the magnetic diffusivity to be exactly zero. Field from the chaotic regions cannot penetrate the islands in the web. If the flow in the islands were completely laminar and there were weak diffusion, field would simply be expelled (Weiss 1966) or amplified by slow dynamo mechanisms (see Soward 1990 and references therein). Although there are likely to be fine bands of chaos within the islands, the chaotic stretching here is very weak, and thus any diffusive leakage of field in and out of the islands is unlikely to affect the growth of field within the chaotic web itself. Another effect of diffusion, absent from our simulations, is to convert components of field along streamlines into transverse field.

Our results may be contrasted and compared with previous studies of laminar and chaotic *ABC* dynamos. The laminar flow with $A = B = 1$ and $C = 0$ (Roberts 1972) is analysed by Soward (1987) and termed a 'nearly fast' dynamo, as the maximum growth rate decreases only as $\ln\ln R_m / \ln R_m$. There is no chaos in the flow, and exponential stretching occurs only at isolated rows of stagnation points. Field transverse to streamlines is stretched out at each row of stagnation points into a fine sheet of flux and then sheared and twisted in the flow (Soward 1987). Now the stretching at stagnation points generates only the field component parallel to streamlines; diffusion acts to convert this back to transverse field and so complete the cycle of field amplification. This diffusive mechanism is absent in our study of chaotic stretching and folding; similarly the chaotic stretching and folding in the flows we have studied is absent in a laminar flow. Our study therefore has little overlap with the analytical study of laminar flows by Soward (1987); the dynamo mechanisms are quite different, and one can only speculate as to how they interact when both are present in a steady chaotic flow at large but finite magnetic Reynolds numbers.

Indeed our results for chaotic flows do differ from those of Soward (1987) for laminar flows in several ways, and have more in common with the studies of Arnold & Korkina (1983) and Galloway & Frisch (1986), who examine the chaotic case $A = B = C = 1$ for magnetic Reynolds numbers up to 550. Soward finds steady growth of magnetic field modes with negative helicity, this being typical of α^2-dynamos. We generally observe oscillatory growth of field, as do Galloway & Frisch (except at very large R_n). We also observe growth of magnetic fields possessing a certain symmetry, independent of their helicity. For example the initial fields in (16) and (17) have the same helicity, being translates of each other, but only one shows clear growth. A similar situation arises in the study of Galloway & Frisch; in the first window of dynamo action the magnetic field has negative helicity in the modes of largest scale, whereas in the second window, after the symmetry breaking, the large-scale field has positive helicity.

Further simulations of dynamo action in *ABC* flows at large but finite magnetic Reynolds numbers would clearly be valuable. A detailed comparison of the field structure between simulations with and without diffusion in this and other steady flows (Galloway & Proctor 1992) could lead to a better understanding of the effects

PHILOSOPHICAL TRANSACTIONS OF THE ROYAL SOCIETY A MATHEMATICAL, PHYSICAL & ENGINEERING SCIENCES

of diffusive reconnection and how it differs from the averaging we have used (see Klapper 1992*b*). Finally, it is important to clarify the rôles of helicity (and its distribution over different scales) and symmetry in these dynamos.

I am grateful to U. Frisch, who suggested this general line of research and, together with S. Childress, made many key contributions during its progress. I have enjoyed many valuable discussions with V. I. Arnold, B. J. Bayly, A. A. Chernikov, D. J. Galloway, I. Klapper, H. K. Moffatt, M. R. E. Proctor, A. V. Rogalsky, S. I. Vainshtein, M. M. Vishik and V. Zheligovsky. I am also grateful to the staff of the Observatoire de Nice, the Courant Institute of Mathematical Sciences and the Woods Hole Oceanographic Institution 1990 Summer Program in Geophysical Fluid Dynamics for their hospitality. This work was supported by Gonville & Caius College, Cambridge, EC contract ST-2J-0029-1-F and NASA contract NAGW-781. S. P. Cooper and the Atmospheric Dynamics Group of D.A.M.T.P. generously made available the software package that was used to produce figure 4.

Appendix A

In §4 it is shown how to move a frozen vector from an initial point in an S-region to a Poincaré section; this appendix gives the modifications required if the initial point lies in an X-region. Define Poincaré sections $P_{\pm}(\boldsymbol{n},\boldsymbol{e})$ in an X-region $X(\boldsymbol{n},\boldsymbol{e})$ by the planes $\pi-\bar{x}=\pm\bar{y}$ in local coordinates $(\bar{x},\bar{y},\bar{z},\boldsymbol{n},\boldsymbol{e})$. Each orbit passing through the X-region intersects one of these planes. The map taking a particle from a section $P(\boldsymbol{n},\boldsymbol{e})$ to one of $P_{\pm}(\boldsymbol{n},\boldsymbol{e})$ is:

$$(\hat{\psi},\hat{\zeta},\hat{\tau},\boldsymbol{n},\boldsymbol{e})=M_{XP}(\psi,\zeta,\tau,\boldsymbol{n},\boldsymbol{e}),$$

where
$$\hat{\psi}=\psi+q(\zeta,\boldsymbol{e}),\quad \hat{\zeta}=\zeta+\tfrac{1}{2}\Delta(\hat{\psi}),\quad \hat{\tau}=\tau+\tfrac{1}{2}T(\hat{\psi}).$$

The particle lands on $P_{+}(\boldsymbol{n},\boldsymbol{e})$ if $\hat{\psi}>0$, otherwise it lands on $P_{-}(\boldsymbol{n},\boldsymbol{e})$.

Now omit the carets and suppose that a particle crosses P_{+} or P_{-} with coordinates $(\psi,\zeta,\tau,\boldsymbol{n},\boldsymbol{e})$; if the particle still lies in the X-region at time t its position in local cartesian coordinates at this time is given by

$$(\bar{x},\bar{y},\bar{z},\boldsymbol{n},\boldsymbol{e})=M^{(t)}_{LX}(\psi,\zeta,\tau,\boldsymbol{n},\boldsymbol{e}),$$

with $\bar{x}=\pi-d(\psi)\,e^{-}(t-\tau)/\gamma,\quad \bar{y}=f(\psi)\,d(\psi)\,e^{+}(t-\tau)/\gamma,\quad \bar{z}=\zeta+(t-\tau)\sqrt{2\psi},$

where $d(\psi)=\sqrt{|\gamma\psi|},\quad e^{+}(t)=1/e^{-}(t)=\exp(\gamma t),\quad f(\psi)=\operatorname{sign}(\psi).$

If a particle travels from an initial point $\boldsymbol{x}_0$ in an X-region, to the point $\boldsymbol{x}$ in an S-region at time t, then

$$\boldsymbol{x}(\boldsymbol{x}_0)=M_{CL}\circ M^{(t)}_{LP}\circ(M_{PP})^{n}\circ(M_{XP})^{-1}\circ(M^{(0)}_{LX})^{-1}\circ(M_{CL})^{-1}\,\boldsymbol{x}_0 \tag{A 1}$$

analogously to (12). Similar formulae apply for particles travelling from an S-region or X-region to an X-region. Differentiating

$$\partial\boldsymbol{x}/\partial\boldsymbol{x}_0=\boldsymbol{J}_{CL}\cdot\boldsymbol{J}^{(t)}_{LP}\cdot(\boldsymbol{J}_{PP})^{n}\cdot(\boldsymbol{J}_{XP})^{-1}\circ(\boldsymbol{J}^{(0)}_{LX})^{-1}\cdot(\boldsymbol{J}_{CL})^{-1}, \tag{A 2}$$

the new jacobians being given by

$$\boldsymbol{J}_{XP}=\frac{\partial(\hat{\psi},\hat{\zeta},\hat{\tau})}{\partial(\psi,\zeta,\tau)}=\begin{pmatrix}1 & q' & 0\\ \frac{1}{2}\Delta' & 1+\frac{1}{2}\Delta' q' & 0\\ \frac{1}{2}T' & \frac{1}{2}T' q' & 1\end{pmatrix}$$

and
$$\boldsymbol{J}^{(t)}_{LX}=\frac{\partial(\bar{x},\bar{y},\bar{z})}{\partial(\psi,\zeta,\tau)}=\begin{pmatrix}-fe^{-}/2d & 0 & -de^{-}\\ e^{+}/2d & 0 & -fde^{+}\\ (t-\tau)\sqrt{2} & 1 & -\sqrt{2\psi}\end{pmatrix}.$$

Table 2. *Character table for the symmetry group of the ABC flow with* $A = B = C = 1$

$\chi(g)$	E	C_3	C_4^2	C_2	C_4
I	1	1	1	1	1
II	1	1	1	−1	−1
III	2	−1	2	0	0
IV	3	0	−1	1	−1
V	3	0	−1	−1	1

Appendix B

This appendix gives the time-preserving symmetries of the *ABC* flow in the case $A = B = C = 1$, when the symmetry group is isomorphic to the symmetry group of the cube without reflections (Arnold & Korkina 1983; Arnold 1984; Dombre *et al.* 1986). The group contains the elements

$$
\begin{aligned}
i(\boldsymbol{x}) &= (x, y, z), & e(\boldsymbol{x}) &= (-z, \pi - x, y + \pi),\\
a(\boldsymbol{x}) &= (\tfrac{1}{2}\pi - y, x + \tfrac{1}{2}\pi, z - \tfrac{1}{2}\pi), & e^2(\boldsymbol{x}) &= (\pi - y, z + \pi, -x),\\
a^2(\boldsymbol{x}) &= (-x, \pi - y, z + \pi), & f(\boldsymbol{x}) &= (z + \pi, -x, \pi - y),\\
a^3(\boldsymbol{x}) &= (y - \tfrac{1}{2}\pi, \tfrac{1}{2}\pi - x, z + \tfrac{1}{2}\pi), & f^2(\boldsymbol{x}) &= (-y, \pi - z, x + \pi),\\
b(\boldsymbol{x}) &= (x - \tfrac{1}{2}\pi, \tfrac{1}{2}\pi - z, y + \tfrac{1}{2}\pi), & g(\boldsymbol{x}) &= (\pi - z, x + \pi, -y),\\
b^2(\boldsymbol{x}) &= (x + \pi, -y, \pi - z), & g^2(\boldsymbol{x}) &= (y + \pi, -z, \pi - x),\\
b^3(\boldsymbol{x}) &= (x + \tfrac{1}{2}\pi, z - \tfrac{1}{2}\pi, \tfrac{1}{2}\pi - y), & h(\boldsymbol{x}) &= (\tfrac{1}{2}\pi - x, z + \tfrac{1}{2}\pi, y - \tfrac{1}{2}\pi),\\
c(\boldsymbol{x}) &= (z + \tfrac{1}{2}\pi, y - \tfrac{1}{2}\pi, \tfrac{1}{2}\pi - x), & j(\boldsymbol{x}) &= (z - \tfrac{1}{2}\pi, \tfrac{1}{2}\pi - y, x + \tfrac{1}{2}\pi),\\
c^2(\boldsymbol{x}) &= (\pi - x, y + \pi, -z), & k(\boldsymbol{x}) &= (y + \tfrac{1}{2}\pi, x - \tfrac{1}{2}\pi, \tfrac{1}{2}\pi - z),\\
c^3(\boldsymbol{x}) &= (\tfrac{1}{2}\pi - z, y + \tfrac{1}{2}\pi, x - \tfrac{1}{2}\pi), & l(\boldsymbol{x}) &= (-x - \tfrac{1}{2}\pi, -z - \tfrac{1}{2}\pi, -y - \tfrac{1}{2}\pi),\\
d(\boldsymbol{x}) &= (z, x, y), & m(\boldsymbol{x}) &= (-z - \tfrac{1}{2}\pi, -y - \tfrac{1}{2}\pi, -x - \tfrac{1}{2}\pi),\\
d^2(\boldsymbol{x}), &= (y, z, x) & n(\boldsymbol{x}) &= (-y - \tfrac{1}{2}\pi, -x - \tfrac{1}{2}\pi, -z - \tfrac{1}{2}\pi);
\end{aligned}
$$

note that the elements b^3 and d^2 correspond to the elements g_4 and g_3 of Arnold (1984).

There are five conjugacy classes,

$$
\begin{aligned}
E &= \{i\}, \quad C_3 = \{d, d^2, e, e^2, f, f^2, g, g^2\}, \quad C_4^2 = \{a^2, b^2, c^2\},\\
C_2 &= \{h, j, k, l, m, n\}, \quad C_4 = \{a, a^3, b, b^3, c, c^3\},
\end{aligned}
$$

and the character table is given in table 2 (see, for example, Hamermesh 1962). In the case $A = B \neq C$, the symmetry group is reduced to D_8, containing the elements $\{i, a, a^2, a^3, b^2, k, c^2, n\}$. Finally if A, B and C are all unequal, the symmetry group is D_4 and contains the elements i, a^2, b^2 and c^2, which correspond to the symmetries I, S_2S_1, S_3S_2 and S_1S_3, respectively, of Dombre *et al.* (1986).

References

Arnold, V. I. 1965 Sur la topologie des écoulements stationnaires des fluides parfaits. *C.r. hebd. Seanc. Acad. Sci., Paris* **261**, 17–20.

Arnold, V. I. 1984 On the evolution of magnetic field under the action of advection and diffusion. In *Some questions of present-day analysis* (ed. V. M. Tikhomirov), pp. 8–21. Moscow University Press. (In Russian.)

Arnold, V. I. & Korkina, E. I. 1983 The growth of a magnetic field in a three-dimensional steady incompressible flow. *Vest. Mosk. Un. Ta. Ser. 1, Math. Mec.* **3**, 43–46.

Arnold, V. I., Zeldovich, Ya. B., Ruzmaikin, A. A. & Sokoloff, D. D. 1981 A magnetic field in a stationary flow with stretching in Riemannian space. *Zh. Eksp. Teor. Fiz.* **81**, 2052–2058. (*Sov. Phys. JETP* **54**, 1083–1086.)

Bayly, B. J. 1986 Fast magnetic dynamos in chaotic flow. *Phys. Rev. Lett.* **57**, 2800–2803.

Bayly, B. J. & Childress, S. 1988 Construction of fast dynamos using unsteady flows and maps in three dimensions. *Geophys. Astrophys. Fluid Dyn.* **44**, 211–240.

Bayly, B. J. & Childress, S. 1989 Unsteady dynamo effects at large magnetic Reynolds number. *Geophys. Astrophys. Fluid Dyn.* **49**, 23–43.

Beloshapkin, V. V., Chernikov, A. A., Natenzon, M. Ya., Petrovichev, B. A., Sagdeev, R. Z. & Zaslavsky, G. M. 1989 Chaotic streamlines in pre-turbulent states. *Nature, Lond.* **337**, 133–137.

Childress, S. 1970 New solutions of the kinematic dynamo problem. *J. Math. Phys.* **11**, 3063–3076.

Childress, S. & Klapper, I. 1991 On some transport properties of baker's maps. *J. statist. Phys.* **63**, 897–914.

Childress, S. & Soward, A. M. 1985 On the rapid generation of magnetic fields. In *Chaos in astrophys.* (ed. J. R. Buchler, J. M. Perdang & E. A. Spiegel), pp. 223–244. Reidel.

Chirikov, B. K. 1979 A universal instability of many-dimensional oscillator systems. *Phys. Rep.* **52**, 263–379.

Cowling, T. G. 1934 The magnetic field of sunspots. *Mon. Not. R. astr. Soc.* **94**, 39–48.

Dombre, T., Frisch, U., Greene, J. M., Hénon, M., Mehr, A. & Soward, A. M. 1986 Chaotic streamlines in the *ABC* flows. *J. Fluid Mech.* **167**, 353–391.

Dresselhaus, E. & Tabor, M. 1990 The geometry of lagrangian orbits. In *Proc. I.U.T.A.M. Symp. on Topological fluid mechanics*, pp. 75–84. Cambridge University Press.

Finn, J. M., Hanson, J. D., Kan, I. & Ott, E. 1991 Steady fast dynamo flows. *Physics Fluids* B **3**, 1250–1269.

Finn, J. M. & Ott, E. 1988 Chaotic flows and fast magnetic dynamos. *Physics Fluids* **31**, 2992–3011.

Finn, J. M. & Ott, E. 1990 The fast kinematic magnetic dynamo and the dissipationless limit. *Physics Fluids* B **2**, 916–926.

Galloway, D. J. & Frisch, U. 1986 Dynamo action in a family of flows with chaotic streamlines. *Geophys. Astrophys. Fluid Dyn.* **36**, 58–83.

Galloway, D. J. & Proctor, M. R. E. 1992 Numerical calculations of fast dynamos for smooth velocity fields with realistic diffusion. *Nature, Lond.* (In the press.)

Gilbert, A. D. 1988 Fast dynamo action in the Ponomarenko dynamo. *Geophys. Astrophys. Fluid Dyn.* **44**, 214–258.

Gilbert, A. D. 1991 Fast dynamo action in a steady chaotic flow. *Nature, Lond.* **350**, 483–485.

Gilbert, A. D. & Childress, S. 1990 Evidence for fast dynamo action in a chaotic web. *Phys. Rev. Lett.* **65**, 2133–2136.

Hamermesh, M. 1962 *Group theory*. Addison-Wesley.

Hénon, M. 1966 Sur la topologie des lignes de courant dans un cas particulier. *C.r. hebd. Seanc. Acad. Sci., Paris* **262**, 312–314.

Klapper, I. 1991 Chaotic fast dynamos. Ph.D. thesis, C.I.M.S., New York University, U.S.A.

Klapper, I. 1992*a* Shadowing and the rôle of small diffusivity in the chaotic advection of scalars. *Phys. Fluids* A. (In the press.)

Klapper, I. 1992*b* On fast dynamo action in chaotic helical cells. *J. Fluid Mech.* (In the press.)

Krause, F. & Rädler, K.-H. 1980 *Mean-field magnetohydrodynamics and dynamo theory*. Oxford: Pergamon Press.

Moffatt, H. K. 1969 The degree of knottedness of tangled vortex lines. *J. Fluid Mech.* **35**, 117–129.

Moffatt, H. K. 1978 *Magnetic field generation in electrically conducting fluids*. Cambridge University Press.

Moffatt, H. K. & Proctor, M. R. E. 1985 Topological constraints associated with fast dynamo action. *J. Fluid Mech.* **154**, 493–507.

PHILOSOPHICAL TRANSACTIONS OF THE ROYAL SOCIETY A MATHEMATICAL, PHYSICAL & ENGINEERING SCIENCES

Otani, N. J. 1988 Computer simulation of fast kinematic dynamos. *Trans. Am. geophys. Un.* **69**, 1366. (Abstract no. SH51-15.)

Parker, E. N. 1979 *Cosmical magnetic fields*. Oxford: Clarendon Press.

Plante, J. F. & Thurston, W. P. 1972 Anosov flows and the fundamental group. *Topology* **11**, 147–150.

Roberts, G. O. 1972 Dynamo action of fluid motions with two-dimensional periodicity. *Phil. Trans. R. Soc. Lond.* A **271**, 411–454.

Roberts, P. H. 1967 *An introduction to magnetohydrodynamics*. New York: Elsevier.

Soward, A. M. 1987 Fast dynamo action in a steady flow. *J. Fluid Mech.* **180**, 267–295.

Soward, A. M. 1990 A unified approach to a class of slow dynamos. *Geophys. Astrophys. Fluid Dyn.* **53**, 81–107.

Soward, A. M. & Childress, S. 1990 Large magnetic Reynolds number dynamo action in a spatially periodic flow with mean motion. *Phil. Trans. R. Soc. Lond.* A **331**, 649–733.

Vainshtein, S. I. & Zeldovich, Ya. B. 1972 Origin of magnetic fields in astrophysics. *Sov. Phys. Usp.* **15**, 159–172.

Vishik, M. M. 1989 Magnetic field generation by the motion of a highly conducting fluid. *Geophys. Astrophys. Fluid Dyn.* **48**, 151–167.

Weiss, N. O. 1966 The expulsion of magnetic flux by eddies. *Proc. R. Soc. Lond.* A **293**, 310–328.

Zaslavsky, G. M., Sagdeev, R. Z. & Chernikov, A. A. 1988 Stochastic nature of streamlines in steady-state flow. *Zh. Eksp. Teor. Fiz.* **94**, 102–115. (*Sov. Phys. JETP* **67**, 270–277.)

Zeldovich, Ya. B. 1957 The magnetic field in the two-dimensional motion of a conducting turbulent fluid. *Sov. Phys. JETP* **4**, 460–462.

Zeldovich, Ya. B., Molchanov, S. A., Ruzmaikin, A. A. & Sokolov, D. D. 1988 Intermittency, diffusion and generation in a nonsteady random medium. *Sov. Sci. Rev. C. Math. Phys.* **7**, 1–110.

Zeldovich, Ya. B., Ruzmaikin, A. A. & Sokoloff, D. D. 1983 *Magnetic fields in astrophysics*. Gordon and Breach.

Received 9 July 1991; accepted 14 October 1991

PHILOSOPHICAL TRANSACTIONS OF THE ROYAL SOCIETY A MATHEMATICAL, PHYSICAL & ENGINEERING SCIENCES

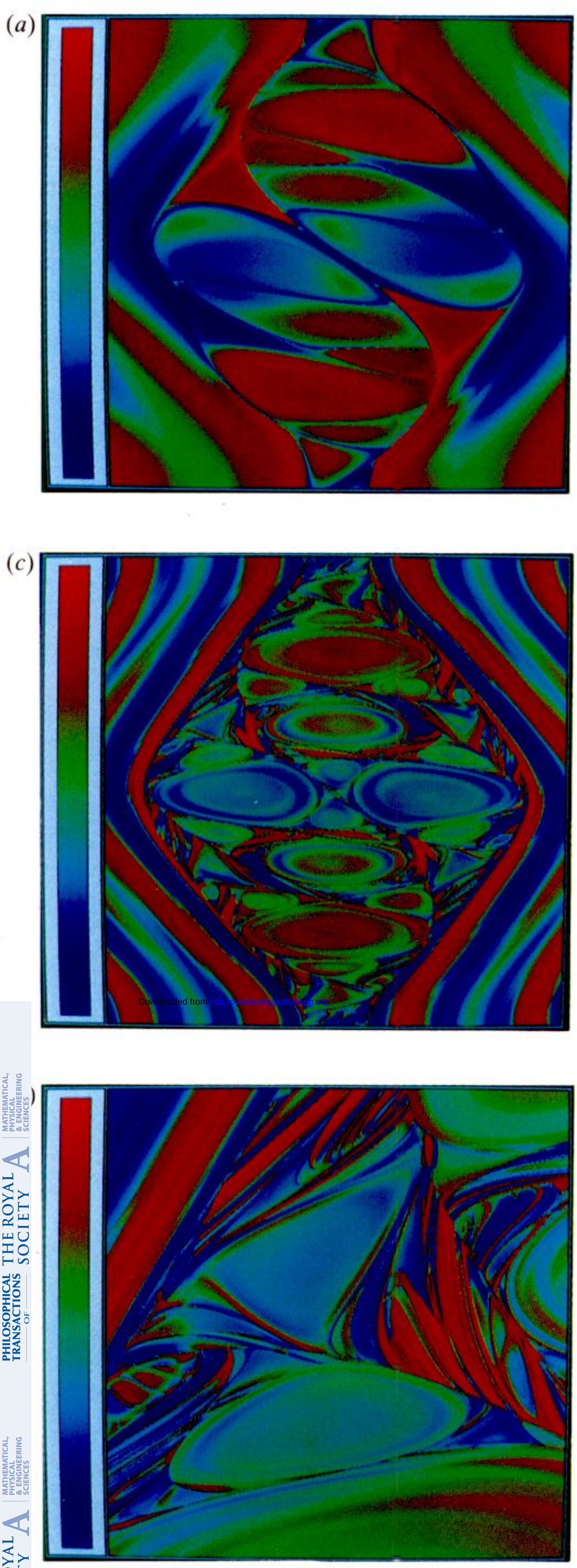

igure 4. Evolution of magnetic field from the initial condition (16). In (*a–c*) the area of $(0,\boldsymbol{e}_x)$ shown is that depicted in figure 3*a* while in (*d–f*) it is that in figure 3*b*. The vertical agnetic field B_z is coded as described in the text, with positive B_z shown in red and egative in blue. In (*a*) $t = 20$, (*b*) $t = 50$, (*c*) $t = 90$, (*d*) $t = 90$, (*e*) $t = 130$ and (*f*) $t = 180$.